Identified Kaon Production in Hadron-Hadron Collisions

Siddha Hill

Matr.Nr. 442132

`siddha.hill@uni-muenster.de`

First examiner: Priv.-Doz. Dr. Karol Kovarik

Second examiner: Prof. Dr. Anna Kulesza

Declaration of Academic Integrity

I hereby confirm that this thesis on the *Identified Kaon Production in Hadron-Hadron Collisions* is solely my own work and that I have used no sources or aids other than the ones stated. All passages in my thesis for which other sources, including electronic media, have been used, be it direct quotes or content references, have been acknowledged as such and the sources cited.

_____

(date and signature of student)

I agree to have my thesis checked in order to rule out potential similarities with other works and to have my thesis stored in a database for this purpose.

_____

(date and signature of student)

Contents

1. Introduction and Outline

High energy hadron collisions have made remarkable contributions to a better understanding of the content and structure of nuclei, the behaviour of elementary particles and the forces acting between them. The importance of particle productions in hadron-hadron collisions is evident, when we consider that about $75\,\%$ of the total cross section at incoming laboratory momenta $p_{lab} > 5\,(\text{GeV/c})$ are production processes [22].

This thesis aims to show a sanity check for the agreement between the theoretical prediction for the multiplicity and experimental data of a $pp \to (K^+ + K^-)X$ process, taken from Betty Bezverkhny Abelev et al. [1]. From this comparison a statement can be made about the validity of the underlying theory for the given framework conditions. The predicted fractional contribution of all two-to-two processes as functions of p_T is then examined.

To study the production process and to obtain the corresponding theoretical prediction for a cross section, an introduction into the underlying field theory quantum chromodynamics is given. In this context the locally gauge invariant Lagrangian is studied for a general non-abelian SU(N) gauge group. These results allow direct access to the information about the Lagrangian of the SU(3) gauge group, and therefore about the strong interactions in quantum chromodynamics. Reasoning for the perturbative approach is given by the analysis of the running coupling constant α_s, which is sufficiently small for the energies that are being regarded in this thesis. The following section gives a translation of the Lagrangian into the Feynman diagrams with corresponding propagator and vertex factors at tree-level. The study of the kinematics and the cross section for a particle production in hadron-hadron collisions sets groundwork for the numerical evaluation and further comparison to experimental data. The fifth section sets focus on the computation of the invariant matrix elements for two-to-two parton sub-processes of hadron-hadron collisions for massless partons. This thesis discusses the calculation of the invariant squared matrix of the sub-processes $q\bar{q} \to gg$ and $qg \to qg$ in great detail. Section 6 compares the theoretical p_T distribution of the cross section of a charged kaon production, which is numerically evaluated with the application of the Monte Carlo method, to experimental data.

2. Introduction to Quantum Chromodynamics

Quantum chromodynamics is a quantum field theory covering the strong interaction between the constituents of hadronic matter, based on the gauge group SU(3). Hadrons are classified as mesons and baryons composed of a quark-antiquark pair and three quarks (or antiquarks), respectively. There are 6 known flavours of quarks that can be ordered into the doublets

$$\begin{pmatrix} u \\ d \end{pmatrix} \quad \begin{pmatrix} c \\ s \end{pmatrix} \quad \begin{pmatrix} t \\ b \end{pmatrix}$$

with each quark being described by the a Dirac-field. Hence, the fields can be written as

$$q = (q_\varphi) = \begin{pmatrix} q_1 \\ q_2 \\ q_3 \\ q_4 \end{pmatrix} \tag{2.1}$$

or $q_f = (q_{\varphi f})$, where the quark is characterised by the newly introduced flavour index $f = 1, 2, \ldots, N_f$ and $N_f = 6$.

A motivation for the postulate of the unobserved quantum number colour is the explanation of the following two issues. First, there is no particular reason why only qqq and $q\bar{q}$ states are observed i.e. no free particle with fractional charge of $+2/3\,e$ and $-1/3\,e$ for u, c, t and d, s, b-quarks, respectively. Secondly, difficulties occur because the antisymmetric wave functions for particles such as the Δ^{++} baryon with spin $3/2$ and charge $+2\,e$ cannot be constructed. Its wave function $|\Delta^{++}\rangle = |u_\uparrow u_\uparrow u_\uparrow\rangle$ is symmetrical and does not obey Fermi-Dirac statistics, despite being a fermion. Thus, a new degree of freedom - described by the quantum number colour - is introduced, which makes $|\Delta^{++}\rangle = \epsilon^{ijk} |u_{i\uparrow} u_{j\uparrow} u_{k\uparrow}\rangle$ antisymmetric with respect to an interchange of two quarks. This new quantum number leads to an additional colour index $i = 1, 2, 3$. Quarks are now represented by $q_{\alpha f i}$. It is of importance that an additional condition is formulated, which states that only colour singlet states are physical [6, p. 1]. In other words, observed particles are 'white' or 'colourless', which explains the association of colour indices with the three additive colours red, green and blue. The corresponding anti-colours (anti-red, anti-green and anti-blue) are demanded due to the fulfilment of colour charge conservation.

The colour singlet states and the corresponding hadrons are

$$q_i q^{-i} \qquad\qquad\qquad \text{mesons}$$
$$\epsilon^{ijk} q_i q_j q_k \qquad\qquad\qquad \text{baryons}$$

and

$$\epsilon_{ijk} q^{-i} q^{-j} q^{-k} \qquad\qquad\qquad \text{antibaryons}$$

with the totally antisymmetric tensor ϵ^{ijk}.

2.1. Short Review of Symmetry and Groups

Particle interactions follow gauge symmetries, which are associated with locally conserved quantities like colour in quantum chromodynamics. The interactions are encoded in the Lagrangian of the system. Occurring terms are identified with vertex factors and propagators. To be more precise, propagators are associated with terms that are quadratic in fields, while the remaining terms are vertex factors. Motivation for the approach to derive Feynman rules is given in section 3. Prerequisites for this discussion are the gauge theories and therewith symmetries. Symmetries are of great interest because they are closely linked to conservation laws. Symmetries are transformations of a state which do not alter the observed quantity. Their presence indicates that the absolute value of a physical quantity is not measurable [13, p. 315].

For instance, the consequence of a continuous translation symmetry is that the absolute position in space cannot be determined. Similarly, it is not possible to measure the absolute phase of a complex field describing an electron. Therefore, the phase can be chosen as an arbitrary value α. The chosen value applies to every point in space because phase differences are measurable (see Aharonov-Bohm effect [2]). Global gauge transformations maintain an invariant Lagrangian when the parameter α is freely chosen and determined for every point in space-time.

If the transformation depends on an arbitrary value $\alpha(x)$, chosen independently at every x in space-time while the Lagrangian remains invariant, it is called a local gauge symmetry. As stated above we try to obtain the Feynman rules and properties of QCD

from a local gauge invariant Lagrangian. The QCD-Lagrangian is going to be formulated in section 2.3 after a brief review of groups. By imposing a SU(N) symmetry on the Lagrangian of a Dirac-field, we introduce gauge fields which are coupled to the particles.

A group is a set $G = g, h, k, \ldots$ of elements with an operation $\circ$ where all elements fulfil the following axioms:

(i) The group is closed to its operation. For $g, h \in G$ is $g \circ h \in G$.

(ii) Existence of a unit element such that $e \circ g = g \circ e = g$.

(iii) There is an inverse element $g^{-1} \in G$ for each $g \in G$ that satisfies $g^{-1} \circ g = g \circ g^{-1} = e$.

(iv) Associativity $(a \circ b) \circ c = a \circ (b \circ c)$ applies for $\forall a, b, c \in G$.

The group is abelian if $\forall g, h \in G : g \circ h = h \circ g$. Hence, non-commutative groups are called non-abelian.

Lie groups are continuous groups with elements $g = g(\alpha_1, \alpha_2, \ldots \alpha_n)$, where an infinitesimal neighbourhood around g can be defined. The parameters α_j are either real or complex. Operators $U \in G$ where

$$U^\dagger U = U U^\dagger = \mathbb{1} \Rightarrow U^\dagger = U^{-1} \tag{2.2}$$

are called unitary. If G is a strongly continuous one-parameter unitary group (on Hilbert space) the unitary transformation can be written as

$$U(t) = \exp[iAt] \tag{2.3}$$

for all $t \in \mathbb{R}$, with the self-adjoint infinitesimal generator A (Stone's Theorem [12, p. 210]).

In preparation for the study of the underlying symmetry group of QCD, special attention is paid to the unitary group SU(N). This group is a subgroup of transformations consisting of unitary $N \times N$ matrices

$$U = \exp\left[-i \sum_{a=1}^{N^2-1} \alpha_a T_a\right] \quad \text{with} \quad |det\, U|^2 = 1. \tag{2.4}$$

The transformations depend on parameters α_a, with $a = 1, \ldots, N^2 - 1$ for the generators T_a. Since SU(N) is unitary, it is apparent that the generators T_a are hermitian and

$\alpha_a \in \mathbb{R}$. The group is generally non-abelian, with its generators forming the Lie-algebra

$$[T_a, T_b] = i f_{abc} T_c, \tag{2.5}$$

where f_{abc} are the structure constants of the group.

2.2. Non-Abelian Gauge Theory

The Lagrangian of a free Dirac-field is going to be investigated under a global SU(N) symmetry, followed by the extension into a local symmetry, following the idea given by [19, pp. 203–207]. This leads to the formulation of a covariant derivative and gauge fields to maintain the invariance of the Lagrangian under local SU(N) transformations. The demand that the gauge fields should be dynamic fields leads to an additional gauge invariant term, which is associated with the kinetic energy. The Lagrangian

$$\mathcal{L} = \overline{\psi}(x)(i\gamma^\mu \partial_\mu - m)\psi(x) \tag{2.6}$$

for a free Dirac field

$$\psi(x) = \begin{pmatrix} \psi_1(x) \\ \vdots \\ \psi_N(x) \end{pmatrix} \tag{2.7}$$

is invariant under global transformations $U \in$ SU(N). This can be shown with

$$
\begin{aligned}
\psi_i(x) &\longrightarrow \psi'_i(x) = (U\psi(x))_i = U_{ij}\psi_j \\
\Rightarrow \overline{\psi}'_i \left(i\gamma^\mu \partial_\mu - m\right) \psi'_i &= \overline{\psi}_i U^\dagger_{ij}(i\gamma^\mu \partial_\mu - m)U_{jk}\psi_k \\
&= \overline{\psi}_i U^\dagger_{ij} U_{jk}(i\gamma^\mu \partial_\mu - m)\psi_k \\
&= \overline{\psi}_i(i\gamma^\mu \partial_\mu - m)\psi_i
\end{aligned}
\tag{2.8}
$$

since U is unitary. Imposing a local gauge variance with transformations performed by $U(x) \in \mathrm{SU(N)}$

$$U(x) = \exp\left[-i \sum_{a=1}^{N^2-1} \alpha_a(x) T_a\right] \tag{2.9}$$

leads to the introduction of a covariant derivative D_μ, since $U(x)$ does not commute with operator ∂_μ anymore, which causes the Lagrangian to break gauge invariance. With

$$A_\mu := A_\mu^a T_a = \sum_{a=1}^{N^2-1} A_\mu^a T_a \tag{2.10}$$

the covariant derivative reads

$$D_\mu = \partial_\mu - ig A_\mu^a(x) T_a = \partial_\mu - ig A_\mu \tag{2.11}$$

with coupling constant g and $N^2 - 1$ gauge fields to regain an invariant Lagrangian. To obtain the transformation of the gauge field, one can take advantage of the imposed invariance of the Lagrangian. After the substitution of the covariant derivative, the Lagrangian

$$\mathcal{L} = \overline{\psi}(x)(i\gamma^\mu D_\mu - m)\psi(x) \tag{2.12}$$

follows. A transformation of fields and covariant derivative yields

$$\overline{\psi}'_i\left(i\gamma^\mu D'\mu - m\right)\psi'_i = \overline{\psi}_i U_{ij}^\dagger(x)(i\gamma^\mu D'_\mu - m)\psi', \tag{2.13}$$

which means that the transformation must satisfy

$$D'_\mu \psi'(x) \overset{!}{=} U(x) D_\mu \psi(x) = U(x) D_\mu U^\dagger(x) \psi'(x). \tag{2.14}$$

Inserting eq. (2.11) gives

$$\begin{aligned}
&(\partial_\mu - ig A'_\mu(x))\psi'(x) = U(x)(\partial_\mu - ig A_\mu(x)) U^\dagger(x)\psi'(x) \\
&\Leftrightarrow \left[(\partial_\mu - ig A'_\mu(x)) - (U(x)(\partial_\mu - ig A_\mu(x)) U^\dagger(x))\right]\psi'(x) = 0,
\end{aligned} \tag{2.15}$$

and therewith the transformation

$$\Rightarrow A'_\mu(x) = U(x)A_\mu U^\dagger(x) + \frac{i}{g}U(x)\partial_\mu U^\dagger(x) \tag{2.16}$$

for the gauge fields, after applying product rule and demanding that eq. (2.15) holds for all $\psi'(x)$. It is sufficient to investigate infinitesimal transformations, if SU(N) is an element of the Lie group. The transformation $U(x)$ becomes

$$U(x) = \mathbb{1} - i\alpha_a(x)T_a \tag{2.17}$$

along with the transformations

$$\psi'(x) = \psi(x) - i\alpha_a(x)T_a\psi(x) \tag{2.18}$$

$$A'_\mu(x) = A_\mu(x) - i\alpha_a(x)\left[T_a, A_\mu(x)\right] - \frac{1}{g}\alpha_a(x)T_a \tag{2.19}$$

$$\Rightarrow A'^a_\mu T_a = A^a_\mu(x)T_a - i\alpha_a(x)A^b_\mu f_{abc}T_c - \frac{1}{g}\alpha_a(x)T_a$$

$$= \left(A^a_\mu + \alpha_b A^c_\mu f_{bca} - \frac{1}{g}\partial_\mu \alpha_a\right)T_a \tag{2.20}$$

for the Dirac and gauge field. The commutator depends on the generators of the Lie-algebra from eq. (2.5), since $A_\mu = A^a_\mu T_a$. If the gauge field is a dynamic property with an associated kinetic energy, an additional locally gauge invariant term

$$\mathcal{L}_{kin} = -\frac{1}{4}F^a_{\mu\nu}F^{\mu\nu}_a \tag{2.21}$$

must be added to the Lagrangian, which depends on field strength tensors $F^a_{\mu\nu}$. The relation

$$\begin{aligned}
F_{\mu\nu} &= \frac{i}{g}\left[D_\mu, D_\nu\right] \\
&= \partial_\mu A_\nu - \partial_\nu A_\mu - ig\left[A_\mu, A_\nu\right] \\
&= \partial_\mu A^a_\nu T_a - \partial_\nu A^a_\mu T_a + gA^a_\mu A^b_\mu f_{abc}T_c \\
&= (\partial_\mu A^a_\nu - \partial_\nu A^a_\mu + gA^b_\mu A^c_\mu f_{bca})T_a \\
&:= F^a_{\mu\nu}T_a
\end{aligned} \tag{2.22}$$

between the covariant derivative and the field strength tensor can be found, and a field strength tensor $F_{\mu\nu}^a$ is defined. The field strength tensor transforms under local gauge transformations $U(x) \in \text{SU(N)}$ as follows:

$$
\begin{aligned}
F_{\mu\nu}' &= \frac{i}{g} \left[D_\mu', D_\nu' \right] \\
&= \frac{i}{g} \left[U(x) D_\mu U^\dagger(x), U(x) D_\nu U^\dagger(x) \right] \\
&= U(x) F_{\mu\nu} U^\dagger(x).
\end{aligned}
\tag{2.23}
$$

2.3. QCD Symmetry Group and Lagrangian

This section studies the construction of the Lagrangian and imposes a local gauge symmetry due to colour conservation, which then applies the results from section 2.2 for this given quantum field theory based on gauge group SU(3). An intuitive approach for the invariance of interactions under rotations in colour space is that the quantum number colour itself is not observed due to colour conservation. The Lagrangian for free quarks was already discussed in the previous section since quarks are spin $1/2$ particles and therefore fermions which obey Fermi-Dirac-statistics. The Lagrangian for free quarks reads therefore

$$
\mathcal{L} = \sum_{i,f} \overline{q}_{if} (i\gamma^\mu \partial_\mu - m_f) q_{if},
\tag{2.24}
$$

where the sum over colour index i and flavour index f is written explicitly while the spinor index φ is suppressed due to an improved legibility. The invariance under local gauge transformations is shown in eq. (2.8). Since the group elements depend on a set of continuous parameters, we identify SU(3) as Lie group with dimension $8 = 3^2 - 1$ due to the eight generators. By applying

$$
\det\left\{ e^A \right\} = e^{\text{Tr}\{A\}}
\tag{2.25}
$$

and the condition $\det\{U\} = 1$, it is clear that

$$
\text{Tr}\{T_a\} = 0.
\tag{2.26}
$$

A realization of the traceless, hermitian generators T_a is given by the linear independent Gell-Mann-matrices $T_a = \lambda_a/2$, which are often referred to as a generalisation of the Pauli-matrices in three-dimensional space with

$$
\lambda_1 = \begin{pmatrix} 0 & 1 & 0 \\ 1 & 0 & 0 \\ 0 & 0 & 0 \end{pmatrix}, \quad
\lambda_2 = \begin{pmatrix} 0 & -i & 0 \\ i & 0 & 0 \\ 0 & 0 & 0 \end{pmatrix}, \quad
\lambda_3 = \begin{pmatrix} 1 & 0 & 0 \\ 0 & -1 & 0 \\ 0 & 0 & 0 \end{pmatrix}
$$

$$
\lambda_4 = \begin{pmatrix} 0 & 0 & 1 \\ 0 & 0 & 0 \\ 1 & 0 & 0 \end{pmatrix}, \quad
\lambda_5 = \begin{pmatrix} 0 & 0 & -i \\ 0 & 0 & 0 \\ -i & 0 & 0 \end{pmatrix}, \quad
\lambda_6 = \begin{pmatrix} 0 & 0 & 0 \\ 0 & 0 & 1 \\ 0 & 1 & 0 \end{pmatrix} \tag{2.27}
$$

$$
\lambda_7 = \begin{pmatrix} 0 & 0 & 0 \\ 0 & 0 & -i \\ 0 & -i & 0 \end{pmatrix}, \quad
\lambda_8 = \frac{1}{\sqrt{3}} \begin{pmatrix} 1 & 0 & 0 \\ 0 & 1 & 0 \\ 0 & 0 & -2 \end{pmatrix}.
$$

The algebra of the group is defined by the relationship

$$
[T_a, T_b] = i f_{abc} T_c \tag{2.28}
$$

between the generators, with structure constants

$$
f_{abc} = -2i \operatorname{Tr}\{[T_a, T_b]\, T_c\}, \tag{2.29}
$$

which are antisymmetric under exchange of any pair of indices. The eight gauge fields are denoted as gluon fields with field strength tensor

$$
G^a_{\mu\nu} = \partial_\mu A^a_\nu - \partial_\nu A^a_\mu + g_s f_{abc} A^b_\mu A^c_\nu \tag{2.30}
$$

transforming according to eq. (2.16). The QCD-Langrangian reads therefore

$$\mathcal{L}_{QCD} = \bar{q}(i\gamma^\mu D_\mu - m)q - \frac{1}{4}G^a_{\mu\nu}G^{\mu\nu}_a \tag{2.31}$$

$$= \bar{q}(i\gamma^\mu \partial_\mu - m)q - g_s\bar{q}\gamma^\mu A^a_\mu T_a q - \frac{1}{4}G^a_{\mu\nu}G^{\mu\nu}_a \tag{2.32}$$

as a sum of the Lagrangian for free quarks and the gauge invariant kinetic energy term for the dynamic gluon field. The final Lagrange density is given by

$$\mathcal{L} = \mathcal{L}_{QCD} + \mathcal{L}_{gauge-fixing} + \mathcal{L}_{ghost}, \tag{2.33}$$

in which the two additional terms are motivated by the fact that the propagator for the gluon field cannot be defined without a choice of gauge and ghost fields cancel out unphysical degrees of freedom such as a polarisation along the direction of propagating gluons [6, p. 8]. The sum over flavour indices is implied in these equations. Gluons have no mass contribution in the Lagrangian, they are therefore massless. An additional term involving the gluon-mass cannot exist, because it would violate the gauge invariance. As a result of the multiplication of the field strength tensors, interesting consequences are observed in QCD. In order to get a first idea of these consequences, it is best to reconstruct the Lagrangian into a symbolic form

$$\mathcal{L}_{QCD} = \text{``}\bar{q}q + g_s\bar{q}qA + A^2 + g_sA^3 + g_s^2A^4\text{''}, \tag{2.34}$$

which highlights participating particles in possible interactions. By looking at the first and third term, which are quadratic in fields, it is clear that freely propagating quarks and gluons are described. Terms that are interpreted to express particle interactions contain the strong coupling constant g_s. Consequently, quark-antiquark-gluon interactions are seen in the second term. In great contrast to quantum electrodynamics, self-interactions between gluons are noticed in the fourth and fifth term. This self-coupling is caused by gluons carrying colour charge. It is unique since it has no analogue to photons in QED.

2.3.1. Comparison to QED

To enable a comparison, we study the QED Lagrangian

$$\mathcal{L} = \overline{\psi}(x)(i\gamma^{\mu}\partial_{\mu} - m)\psi(x) \tag{2.35}$$

following the same procedure as in the previous section. The Lagrangian of quantum electrodynamics is based on a $U(1)$ symmetry, since the absolute phase of a complex field is not measurable. The transformation operators

$$U = e^{-iq\alpha} \tag{2.36}$$

are commutative, and form an abelian group in contrast to the previous section. The global gauge invariance of the Lagrangian under these transformations can be seen from eq. (2.8). A local transformation

$$U(x) = e^{-iq\alpha(x)} \tag{2.37}$$

requires the covariant derivative

$$D_{\mu} = \partial_{\mu} + iqA_{\mu}(x) \tag{2.38}$$

with coupling constant q, which transforms as seen in eq. (2.14) and introduces the gauge field (photon field), which obeys the gauge transformations given in eq. (2.16). The dynamic gauge field adds the invariant term

$$\mathcal{L}_A = -\frac{1}{4}F_{\mu\nu}F^{\mu\nu} \tag{2.39}$$

with

$$F_{\mu\nu} \overset{eq. \ (2.22)}{=} \partial_{\mu}A_{\nu} - \partial_{\nu}A_{\mu}, \tag{2.40}$$

which gives the QED-Lagrangian

$$\mathcal{L}_{QED} = \overline{\psi}(x)(i\gamma^{\mu}D_{\mu} - m)\psi(x) - \frac{1}{4}F_{\mu\nu}F^{\mu\nu}. \tag{2.41}$$

A reconstruction into a symbolic form gives

$$\mathcal{L}_{QED} = \text{``}\overline{\psi}\psi + q\overline{\psi}\psi A + A^2\text{''}. \tag{2.42}$$

The quadratic terms express propagating fermions and gauge particles – the photons – while the interaction of two fermions through a photon is given by the second term. An abelian symmetry group in QED leads to the absence of any self-interaction of gauge particles that were seen in QCD. Both Lagrangians do not contain a "m^2A^2" term, which shows that the gauge bosons are massless due to the gauge invariance.

2.4. Running Coupling Constant: Confinement and Asymptotic Freedom

The characteristic property of the strong coupling constant is the energy dependency of the running coupling constant $\alpha_s(Q^2) = g_s^2(Q^2)/4\pi$ in QCD (see fig. 1), which is a consequence of the self-interaction of gluons [16, p. 15]. It is observed to be large at small energies and small at large energies, which causes the confinement of coloured quarks in hadrons and the asymptotic freedom, for the number of quark flavours $n_f < 16$. The asymptotic freedom justifies the application of perturbation theory in QCD, which considers quasi-free constituents of hadrons at sufficiently high energies and therefore short distance interactions [13, p. 171]. The behaviour of the coupling constant in regards to the momentum transfer $Q^2 := -q^2$ is described by the differential equation

$$Q\frac{d}{dQ}g_s(Q) = \beta(g_s). \tag{2.43}$$

The β-function is a power series where the lowest order approximation is given by

$$Q\frac{d}{dQ}g_s(Q) \approx -\frac{1}{16\pi^2}\left[11 - \frac{2}{3}n_f\right] \cdot g_s^3(Q) \tag{2.44}$$

with n_f quark flavours. Applying the method of separation of variables for solving eq. (2.44) and substituting $g_s^2(Q^2) = 4\pi\alpha_s(Q^2)$ yields

$$\alpha_s(Q^2) = \frac{\alpha_s(\mu^2)}{1 + \frac{1}{4\pi} \cdot (11 - \frac{2}{3}n_f) \cdot \alpha_s(\mu^2) \cdot \ln\left(\frac{Q^2}{\mu^2}\right)}. \tag{2.45}$$

With the introduction of scale-parameter Λ, the coupling constant can be written as

$$\alpha_s(Q^2) = \frac{4\pi}{\left[11 - \frac{2}{3}n_f\right]\ln\left(\frac{Q^2}{\Lambda^2}\right)} = \frac{4\pi}{\beta_0\ln\left(\frac{Q^2}{\Lambda^2}\right)}. \tag{2.46}$$

Λ is used as a boundary for the distinction between strongly bound states and quasi-free particles, which can be studied with perturbative computations. The latter point applies to $Q^2 \gg \Lambda^2$. Thus, bound states (hadrons) are considered for Q^2 in order of Λ^2. The scale-parameter is determined by

$$\Lambda^2 = Q^2 \exp\left\{-\frac{4\pi}{\beta_0\alpha_s(Q^2)}\right\} \tag{2.47}$$

through experiments (see fig. 1). A brief motivation for the colour confinement, and therefore the reason why only 'colourless' particles are observed, will be shown by the simplified example of a meson and the self-interaction between gluons based on the idea from [8, p. 158]. The field that 'bonds' a quark-antiquark pair into a colourless meson can be described by gluonic field lines. In contrast to electrodynamics, where the density of field lines decreases with increasing distance of two particles of opposite charge, a separation of a quark-antiquark pair (of opposite colour) does not lead to a diminishing field line density. This is a consequence of the attraction of field lines due to the self interaction of gluons, which causes them to form a tube of a diameter in order of $1\,\text{fm}$, consisting of almost parallel field lines. Hence, the mediated force is constant, while the potential field energy grows approximately linearly with increasing distance r in the far field according to

$$V(r) \approx -\frac{4}{3} \cdot \frac{\alpha_s(r)}{r} + k \cdot r. \tag{2.48}$$
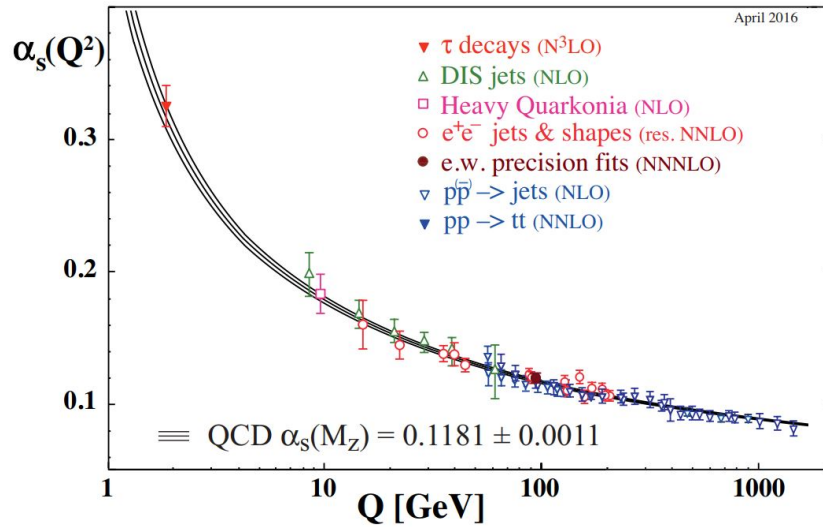
Figure 1: Running coupling constant α_s in theoretical calculation compared to data from different processes as function of energy scale Q. The respective degree of QCD perturbation theory used in the extraction of α_s indicated in brackets (NLO:next-to-leading order; NNLO: next-to-next-to leading order; res.NNLO: NNLO matched with resummed next-to-leading logs;NNNLO (N3LO): next-to-NNLO), taken from [20].

Eventually, it turns out to be energetically favourable to create a corresponding $\bar{q}q$ pair from the vacuum, where the created particles form the new start or endpoint of the significantly shortened gluonic field lines. This Lund string model is the underlying process for the hadronisation of scattered quarks and gluons in high-energy proton-proton collisions.

3. Feynman Rules

The previous section gives a brief introduction of the Lagrangian $\mathcal{L}_{QCD}$ and the asymptotic freedom, leading to the application of perturbative QCD. Perturbation theory can only be performed with the addition of a gauge fixing term, supplemented by a ghost term. This section uses the Lagrangian to derive the Feynman rules, which are represented by graphs displaying the perturbation series of the transition amplitude for a process from the initial to final state following [6, pp. 8–11] and [21, pp. 240–250]. It shows that the Feynman rules can be obtained from the action

$$S = i \int d^4x \mathcal{L}, \tag{3.1}$$

which is the phase of the transition amplitude. A more detailed derivation is given in [21, pp. 182, 250]. Since $\mathcal{L}$ can be decomposed into a non-interacting term $\mathcal{L}_0$ and $\mathcal{L}_I$, which contains the terms describing interactions, the expression

$$S = i \int d^4x \mathcal{L}_0(x) + i \int d^4x \mathcal{L}_I(x) \tag{3.2}$$

follows. The Lagrangian can be written as $\mathcal{L} = \mathcal{L}_0 + \mathcal{L}_I$ where

$$\mathcal{L}_0 = \underbrace{\overline{q}_i \left(i\gamma^\mu \partial_\mu - m \right) q_j}_{\text{quark propagator}} \underbrace{- \frac{1}{2} \partial_\mu A_\nu^a \partial^\mu A_a^\nu + \frac{1}{2} \partial_\nu A_\mu^a \partial^\mu A_a^\nu + \mathcal{L}_{gauge-fixing}}_{\text{gluon propagator}}$$

and

$$\mathcal{L}_I = \underbrace{g_s \overline{q}_i \gamma^\mu A_\mu^a T_a q_j}_{\text{quark-quark-gluon}} + \underbrace{\frac{1}{4} g_s f_{abc} (\partial_\mu A_\nu^a A_b^\mu A_c^\nu - \partial_\nu A_\mu^a A_b^\mu A_c^\nu + A_\mu^b A_\nu^c \partial^\mu A_a^\nu - A_\mu^b A_\nu^c \partial^\nu A_\mu^a)}_{\text{3-gluon interaction}}$$
$$\underbrace{- g_s^2 f^{abc} f_{abc} A_\mu^b A_\nu^c A_b^\mu A_c^\nu}_{\text{4-gluon interaction}} + \underbrace{\mathcal{L}_{ghost}}_{gluon-ghost interaction} . \tag{3.3}$$

The allocations of the interactions to the corresponding terms can be made intuitively by recognising the interacting fields such as the two quark fields $q_{i/j}$, which will be investigated first.

The following method gives the inverse propagator of the corresponding part of $-S_0$ and the vertex factors of the interactions given in S_I, which are treated as perturbations [6, p. 8].

Since one can translate the operator $\partial_\mu = -ip_\mu$ into momentum space, the propagator

$$q_i \longrightarrow q_j \qquad\qquad i\delta_{ij}\frac{1}{\not{p}-m} = i\frac{\not{p}+m}{p^2-m^2} \qquad (3.4)$$

follows. It is interpreted as a quantity of the probability of the particle to propagate at the given energy and momentum. The covariant fixing term for a choice of gauge

$$\mathcal{L}_{\text{gauge-fixing}} = -\frac{1}{2\lambda}\left(\partial_\mu A_a^\mu\right)^2 \qquad (3.5)$$

is chosen accordingly to [6, p. 8] and added to the Lagrangian $\mathcal{L}_0$, which then can be rewritten as

$$\frac{1}{2}A_\mu^a\left[g^{\mu\nu}\Box + \left(1 - \frac{1}{\lambda}\right)\partial^\mu\partial^\nu\right]A_\nu^b, \qquad (3.6)$$
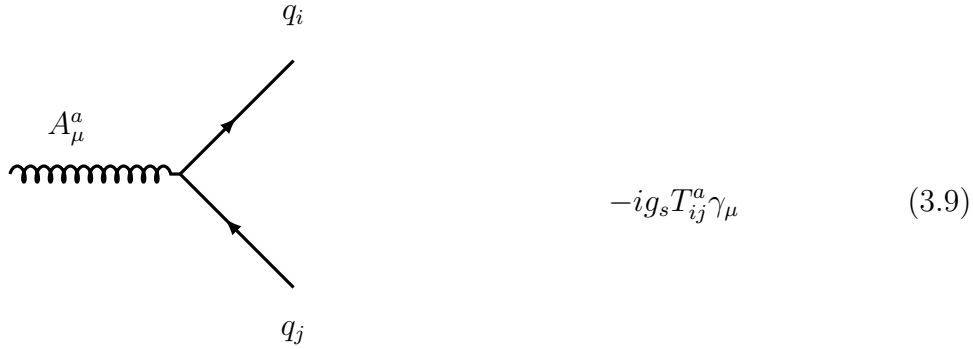
with the d'Alembertian operator $\Box = \partial_\mu\partial^\mu$. In a similar pattern to the latter procedure, the negative, inverse gluon operator can be expressed as

$$i\delta_{cd}\left[p^2 g^{\mu\nu} - \left(1 - \frac{1}{\lambda}\right)p^\mu p^\nu\right]. \qquad (3.7)$$

Hence, the propagator

$$A_c^\mu \qquad\qquad A_d^\nu \qquad\qquad \delta_{cd}\left[-g^{\mu\nu} + (1-\lambda)\frac{p^\mu p^\nu}{p^2}\right]\frac{i}{p^2} \qquad (3.8)$$

follows for an arbitrary parameter λ. In the following calculations the Feynman gauge with $\lambda = 1$ is chosen. The term associated with the vertex of a quark-gluon-quark interaction is taken from the first term of $\mathcal{L}_I$. It follows the vertex factor

$$-ig_s T^a_{ij}\gamma_\mu \qquad (3.9)$$
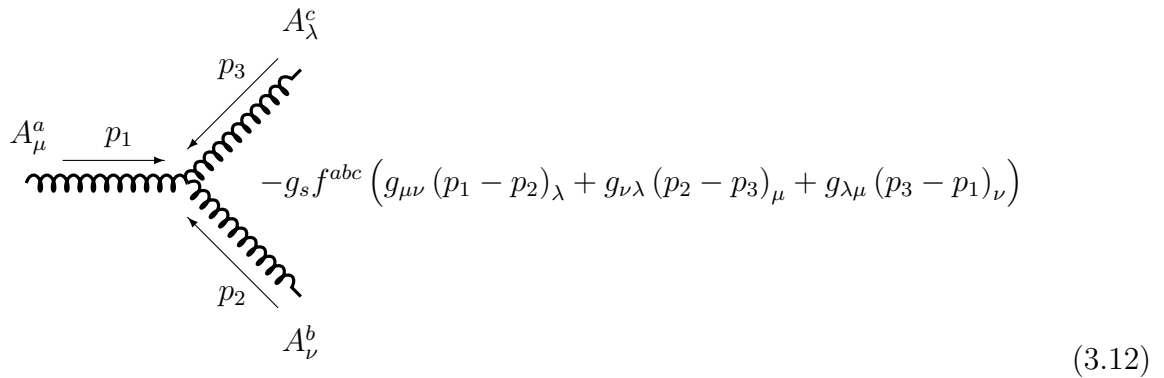
with the corresponding diagram fraction.

The triple gluon vertex

$$\frac{1}{4}g_s f_{abc}(\partial_\mu A^a_\nu A^\mu_b A^\nu_c - \partial_\nu A^a_\mu A^\mu_b A^\nu_c + A^b_\mu A^c_\nu \partial^\mu A^\nu_a - A^b_\mu A^c_\nu \partial^\nu A^a_\mu) \qquad (3.10)$$

can be rewritten as
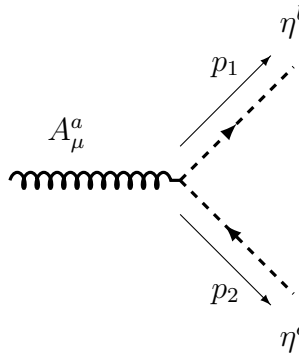
$$if_{abc}\frac{g_s}{2}(g_{\mu\nu}p_{1\lambda} - g_{\lambda\mu}p_{1\nu})A^\mu_a A^\nu_b A^\lambda_c \qquad (3.11)$$

with the substitution of $i\partial_\mu A^\mu_a = p_\mu A^\mu_a$. The summation of eq. (3.10) over all 3! permutations for all possible gluon arrangements gives

$$-g_s f^{abc}\left(g_{\mu\nu}(p_1 - p_2)_\lambda + g_{\nu\lambda}(p_2 - p_3)_\mu + g_{\lambda\mu}(p_3 - p_1)_\nu\right)$$

$$(3.12)$$

for the triple gluon vertex. Finally, the ghost vertex

$$-g_s f^{abc}(p_1)_\mu \qquad (3.13)$$

is introduced, which is a consequence of the additional term

$$\mathcal{L}_{ghost} = \partial_\mu \bar{\eta}^b \partial^\mu \eta^b + g_s f^{abc} \left(\partial^\mu \bar{c}^a\right) A^a_\mu \eta^c \qquad (3.14)$$

to the Lagrangian. The ghost propagator and the 4-gluon vertex will not be reviewed as they do not appear in the explicitly calculated processes in section 5. They can be found along with all the Feynman rules in [18].

4. Kinematics

4.1. Mandelstam Variables and Rapidity

Mandelstam variables describe useful quantities, which are invariant under Lorentz transformations in $1 + 2 \rightarrow 3 + 4$ scattering processes. They are used to replace energies, three-momenta and scattering angle of the interacting particles with

$$
\begin{aligned}
s &= (p_1 + p_2)^2 = (p_3 + p_4)^2 \\
&= m_1^2 + m_2^2 - 2(E_1 E_2 - |\vec{p_1}||\vec{p_2}| \cos \theta_1)
\end{aligned}
\tag{4.1}
$$

$$
\begin{aligned}
t &= (p_1 - p_3)^2 = (p_2 - p_4)^2 \\
&= m_1^2 + m_3^2 - 2(E_1 E_3 - |\vec{p_1}||\vec{p_3}| \cos \theta_2)
\end{aligned}
\tag{4.2}
$$

$$
\begin{aligned}
u &= (p_1 - p_4)^2 = (p_2 - p_3)^2 \\
&= m_1^2 + m_4^2 - 2(E_1 E_4 - |\vec{p_1}||\vec{p_4}| \cos \theta_3).
\end{aligned}
\tag{4.3}
$$

Momentum conservation $p_1 + p_2 = p_3 + p_4$, eqs. (4.1) to (4.3) and the invariant mass $p_i^2 = m_i$ yield the relation

$$
s + t + u = p_1^2 + p_2^2 + p_3^2 + p_4^2 = m_1^2 + m_2^2 + m_3^2 + m_4^2.
\tag{4.4}
$$

It is evident that only two of the three Mandelstam variables are independent. The particles' masses are negligible at sufficiently high energies, which leads to

$$
s \approx 2p_1 \cdot p_2 = 2p_3 \cdot p_4
\tag{4.5}
$$

$$
t \approx -2p_1 \cdot p_3 = -2p_2 \cdot p_4
\tag{4.6}
$$

$$
u \approx -2p_1 \cdot p_4 = -2p_2 \cdot p_3.
\tag{4.7}
$$

Two sets of variables are required to describe hadron-hadron collisions, since hadrons consist of quarks. This is also the reason why the centre-of-mass frame of two colliding partons is typically boosted with regards to the colliding hadron-hadron beams. We denote $s, t, u, \ldots$ and $\hat{s}, \hat{t}, \hat{u}, \ldots$ as variables at hadron- and parton-level, respectively.

The probability of partons to be found with momentum fraction x of the total hadron momentum is described by parton distribution functions (PDF's) $f(x, Q^2)$ at factorisation

scale Q^2. The rapidity

$$y = \frac{1}{2} \ln \frac{E + p_z}{E - p_z} \tag{4.8}$$

is introduced to simplify further calculations for particles with boosts parallel to the z-axis, by being additive for Lorentz transformations and showing boost-invariant differences for two rapidities. A relation between $E_{cm} = \sqrt{s}$ at hadron level and $\sqrt{\hat{s}}$ at parton-level is given by the momentum fractions

$$x_1 = \frac{p_T}{\sqrt{s}} \left(e^{y_3} + e^{y_4} \right) \tag{4.9}$$

and

$$x_2 = \frac{p_T}{\sqrt{s}} \left(e^{-y_3} + e^{-y_4} \right), \tag{4.10}$$

which are a consequence of momentum conservation $\hat{s} = x_1 x_2 s$ for the observed final-state rapidities $y_{3/4}$ and transverse momentum p_T.

The four-momenta of the hadron beams read

$$P_1 = (E_1, 0, 0, P_1), \quad P_2 = (E_1, 0, 0, -P_1), \tag{4.11}$$

which leads to the four-momentum

$$p_{h,cm} = [(x_1 + x_2)E_1, 0, 0, (x_1 - x_2)P_1] \tag{4.12}$$

of the parton-frame, with $x_{1/2}$ being the corresponding fraction of the hadron momentum in the lab frame. The boost of the parton system to the lab frame is therefore given by

$$y = \frac{1}{2} \ln \frac{x_1}{x_2}. \tag{4.13}$$

In the partons' centre-of-mass system, both final state particles scatter back-to-back with a rapidity of

$$\pm \hat{y} = \frac{y_3 - y_4}{2}, \tag{4.14}$$

while the laboratory rapidity of the two outgoing particles is

$$y_{cm} = \frac{y_3 + y_4}{2} \tag{4.15}$$

depending on the observed rapidities $y_{3/4}$. The scattering angle in the parton's centre-of-mass system can be extracted from

$$\cos \hat{y} = \frac{\hat{p}_z}{\hat{E}} = \frac{\sinh \hat{y}}{\cosh \hat{y}} = \tanh \left(\frac{y_3 - y_4}{2} \right). \tag{4.16}$$

With the latter two expressions, the momentum fractions can be rewritten as

$$x_1 = 2p_T e^{y_{cm}} \cosh \hat{y}, \quad x_2 = 2p_T e^{-y_{cm}} \cosh \hat{y}, \tag{4.17}$$

which gives the relation

$$\hat{s} = 4p_T^2 \cosh^2 \hat{y} \tag{4.18}$$

between measurable observables and the square of the parton's centre-of-mass energy. With transverse momentum p_T, azimuthal angle Φ and $E_T = \sqrt{p_T^2 + m^2}$ the four-momentum can be rewritten as

$$p^\mu = (E, p_x, p_y, p_z) = (E_T \cosh y, p_T \sin \Phi, p_T \cos \Phi, E_T \sinh y). \tag{4.19}$$

4.2. Cross Section

A cross section is a quantity of the probability of an interaction, such as absorption, scattering, reaction, etc. between two colliding particles to occur. For instance, a differential cross section $d\sigma/d\Omega$ describes the angular distribution of a scattering process.

The hard scattering of two hadrons is described by the parton model, in which the cross section of particles with incoming four-momenta $P_{1/2,hadron}$ is written as a combination of the short-distance cross section $\hat{\sigma}$ of partons and PDF's $f_i(x, Q^2)$, defined at factorisation scale Q^2. Hence,

$$d\sigma(H_1 H_2 \to H_3 H_4) = \sum_{i,j} \int dx_1 dx_2 f_i(x_1, Q^2) f_j(x_2, Q^2) d\hat{\sigma}(ij \to kl) \tag{4.20}$$

follows with $p_{1/2,parton} = x_{1/2} \cdot P_{1/2,hadron}$ and the characteristic hard scattering scale Q. This expression is integrated over all momentum fractions and summed over all relevant pairs of partons. Since the coupling is small at high energies, the short distance cross section can be evaluated with the application of perturbation theory (see fig. 1). The differential cross section for a two particle interaction via $1 + 2 \to 3 + 4 + \ldots n$ is given by

$$d\hat{\sigma} = \frac{\overline{\sum}|\mathcal{M}|^2}{F} dPS_n, \tag{4.21}$$

where $\overline{\sum}$ corresponds to the average over initial and the sum over final spin and colour states. $F = |\vec{v}_1 - \vec{v}_2| \cdot 2E_1 \cdot 2E_2$ denotes the invariant flux for a general colliniear collision, which ensures a normalisation-independent measure of the initial and final states of the process [13, p. 89]. The flux can be written as

$$F = 4 \cdot \sqrt{E_1^2 E_2^2 \left(\frac{\vec{p}_1}{E_1} + \frac{\vec{p}_2}{E_2}\right)^2} = 4 \cdot |\vec{p}_i|\sqrt{E_1 + E_2} \tag{4.22}$$

$$= 4|\vec{p}_i|\sqrt{\hat{s}} = 2\hat{s} \tag{4.23}$$

for initial momenta $\pm\vec{p}_i$ in the centre-of-mass frame. The Lorentz invariant phase space factor is written as

$$dPS_n = \frac{1}{(2\pi)^{3n-4}} \prod_{l=1}^{n} \frac{d^3\vec{p}_l}{2E_l} \delta^{(4)}\left(p_1 + p_2 - \sum_{l=1}^{n} p_l\right) \tag{4.24}$$

for n final state particles. The Lorentz invariant phase space element for a $1 + 2 \longrightarrow 3 + 4$ scattering process reads

$$dPS_2 = \frac{1}{(2\pi)^2} \frac{d^3\vec{p}_3}{2E_3} \frac{d^3\vec{p}_4}{2E_4} \delta^{(4)}\left(p_1 + p_2 - p_3 - p_4\right)$$

$$\stackrel{eq. (4.26)}{=} \frac{1}{8\pi^2} \frac{d^3\vec{p}_3}{E_3} \delta^{(4)}(p_1 + p_2 - p_3 - p_4) d^4p_4 \delta(p_4^2 - m_4^2) \tag{4.25}$$

$$\stackrel{eq. (4.27)}{=} \frac{1}{8\pi^2} \frac{d^3\vec{p}_3}{E_3} \delta\left(\hat{s} - 2p^0 \cdot p_3^0\right),$$

where the 4-dimensional delta function vanishes due to the integration over the d^4p_4

element. The substitution of

$$\frac{d^3\vec{p}}{2E} = d^4 p \, \delta\left(p^2 - m^2\right) \tag{4.26}$$

and

$$p = p_1 + p_2 = \sqrt{\hat{s}}\left(1, \vec{0}\right), \quad p_3 = \left(\sqrt{\hat{s}}/2, \vec{p}\right), \quad p_4 = \left(\sqrt{\hat{s}}/2, -\vec{p}\right) \tag{4.27}$$

are used for massless particles in the centre-of-mass frame. Hence, the differential short distance cross section

$$\frac{E d\hat{\sigma}}{d^3\vec{p}} = \overline{\sum}|\mathcal{M}|^2 \frac{1}{2\hat{s}} \frac{1}{8\pi^2} \delta\left(\hat{s} - 2p^0 \cdot p_3^0\right) \tag{4.28}$$

follows. To describe a particle production, another modification of the cross section given in eq. (4.20) is implemented. Thus, the hard inelastic cross section of a particle production reads

$$\begin{aligned}
\frac{E_k d^3\sigma}{d^3\vec{p}_k} =& \frac{1}{16\pi^2 s} \sum_{i,j,k,l=q,\bar{q},g} \frac{dx_1}{x_1} \frac{dx_2}{x_2} dx_3 f_i(x_1, Q^2) f_j(x_2, Q^2) D_{h/k}(x_3, \mu^2) \\
&\times \overline{\sum}|\mathcal{M}_{ij \to kl}|^2 \frac{1}{1 + \delta_{ij}} \frac{1}{1 + \delta_{kl}} \delta\left(\hat{s} - 2p^0 \cdot p_3^0\right),
\end{aligned} \tag{4.29}$$

which is the previous cross section accompanied by a fragmentation function $D_{h/k}(x_3, \mu^2)$ and the extension of the sum over all relevant initial and final parton pairs [15, p. 170]. Fragmentation functions represent a measurement of the probability density of parton k to be scattered into a a hadron h with momentum fraction $x_3 = p_h/p_k$, which is transferred from the parton to the hadron. Fragmentation functions can be understood as the final-state analog of initial-state PDF's. It is favourable to rewrite the differential cross section further in terms of transverse momentum p_T and rapidity y to make direct use of experimentally accessible variables which are bound to the experimental setup of

the detector. With

$$\frac{Ed^3\sigma}{d^3\vec{p}} \stackrel{polar}{=} \frac{Ed^3\sigma}{d^2p_T dp_z}$$
$$\stackrel{eq.\ (4.31)}{=} \frac{d^3\sigma}{dy d^2p_T} \tag{4.30}$$
$$= \frac{d^2\sigma}{2\pi p_T dy dp_T},$$

where the relation

$$dp_z \stackrel{eq.\ (4.19)}{=} Edy \tag{4.31}$$

and symmetry in azimuthal angle Φ were used, the differential cross section can be written as

$$\frac{d^6\sigma}{dx_1 dx_2 dx_3 dy_k dp_T^2} = \frac{1}{16\pi^2 \hat{s}} \sum_{i,j,k,l=q,\bar{q},g} f_i(x_1,Q^2) f_j(x_2,Q^2) D_{k/K}(x_3,\mu^2)$$
$$\times \overline{\sum} |\mathcal{M}_{ij\to kl}|^2 \frac{1}{1+\delta_{ij}} \frac{1}{1+\delta_{kl}} \delta\left(x_1 x_2 s - \hat{s}\right) \tag{4.32}$$

with

$$2p^0 p_3^0 = 2\sqrt{\hat{s}} \frac{\sqrt{\hat{s}}}{2}. \tag{4.33}$$

The transformation $x_{1/2} = \sqrt{\tau} e^{\pm y_{cm}}$ of the momentum fractions leads to $dx_1 dx_2 = d\tau dy_{cm}$, and therefore,

$$\frac{d^6\sigma}{dx_3 dy_k d^2 p_T dy_{cm} d\tau} = \frac{1}{16\pi^2 \tau s^2} \sum_{i,j,k,l=q,\bar{q},g} f_i(x_1,Q^2) f_j(x_2,Q^2) D_{h/k}(x_3,\mu^2)$$
$$\times \overline{\sum} |\mathcal{M}_{ij\to kl}|^2 \frac{1}{1+\delta_{ij}} \frac{1}{1+\delta_{kl}} \delta\left(\tau - \hat{s}/s\right), \tag{4.34}$$

where the Dirac-delta function was rewritten $\delta\left(\tau s - \hat{s}\right) = \delta\left(\tau - \hat{s}/s\right)/s$. The integration over $d\tau$ fixes τ to

$$\tau \stackrel{eq.\ (4.9)}{=} \frac{4p_T^2}{s} \cosh^2 \hat{y}, \tag{4.35}$$

which yields

$$\frac{d^5\sigma}{dx_3 dy_k d^2p_T dy_{cm}} = \frac{1}{16\pi^2\tau s^2} \sum_{i,j,k,l=q,\bar{q},g} f_i(x_1, Q^2) f_j(x_2, Q^2) D_{h/k}(x_3, \mu^2)$$
$$\times \overline{\sum} |\mathcal{M}_{ij\to kl}|^2 \frac{1}{1+\delta_{ij}} \frac{1}{1+\delta_{kl}}. \tag{4.36}$$

To gain access to the measured information, another transformation from $y_k y_{cm} \to y_3 y_4$ is given by

$$y_k = \hat{y} = \frac{y_3 - y_4}{2}, \quad y_{cm} = \frac{y_3 + y_4}{2} \tag{4.37}$$

with the Jacobian matrix

$$\det\{J\} = \det\left\{\frac{\partial(y_k, y_{cm})}{\partial(y_3, y_4)}\right\} = \frac{1}{2}. \tag{4.38}$$

Simultaneously $d^2p_T = 2\pi p_T dp_T$ is substituted, which gives

$$\frac{d^4\sigma}{dx_3 dy_3 dy_4 dp_T} = \frac{p_T}{16\pi\tau s^2} \sum_{i,j,k,l=q,\bar{q},g} f_i(x_1, Q^2) f_j(x_2, Q^2) D_{h/k}(x_3, \mu^2)$$
$$\times \overline{\sum} |\mathcal{M}_{ij\to kl}|^2 \frac{1}{1+\delta_{ij}} \frac{1}{1+\delta_{kl}}. \tag{4.39}$$

Since p_T is the transverse momentum of the outgoing partons and energy fraction $x_3 = P_h/p_3 = P_{T,h}/p_T$ of the outgoing hadron h the determinant of the Jacobian matrix of the transformation from $x_3 \to P_{T,h}$ gives

$$\frac{\partial x_3}{\partial P_{T,h}} = 1/p_T. \tag{4.40}$$

Subsequently, the differential cross section

$$\frac{d^4\sigma}{dP_{T,h} dp_T dy_3 dy_4} = \frac{1}{16\pi\tau s^2} \sum_{i,j,k,l=q,\bar{q},g} f_i(x_1, Q^2) f_j(x_2, Q^2) D_{h/k}(x_3, \mu^2)$$
$$\times \overline{\sum} |\mathcal{M}_{ij\to kl}|^2 \frac{1}{1+\delta_{ij}} \frac{1}{1+\delta_{kl}} \tag{4.41}$$

is integrated over the partonic transverse momentum p_T and rapidity dy_3, which leaves a dependency on y_4 and $P_{T,h}$ for comparisons to experimental data. Limits for the integration over transverse momentum of the parton result from $P_{T,h} \leq p_T \leq \sqrt{s}/2$. Rapidity y_3 is bound by

$$p_3 = p_T \cosh y_3, \quad p_4 = p_T \cosh y_4, \quad p_3 + p_4 = \sqrt{s}, \tag{4.42}$$

which gives

$$y_{3,min/max} = \pm \operatorname{arcosh}\left(\frac{\sqrt{s}}{p_T} - \cosh y_4\right), \tag{4.43}$$

and therefore,

$$\begin{aligned}
\frac{d^2\sigma}{dP_{T,h}dy_4} &= \int_{P_{T,h}}^{\frac{\sqrt{s}}{2}} dp_T \int_{y_{3,min}}^{y_{3,max}} dy_3 \frac{1}{16\pi\tau s^2} \sum_{i,j,k,l=q,\bar{q},g} f_i(x_1,Q^2) f_j(x_2,Q^2) D_{h/k}(x_3,\mu^2) \\
&\times \overline{\sum}|\mathcal{M}_{ij\rightarrow kl}|^2 \frac{1}{1+\delta_{ij}} \frac{1}{1+\delta_{kl}}
\end{aligned} \tag{4.44}$$

with $x_{1/2} = x_{1/2}(s, p_T, y_3, y_4)$ and $x_3 = x_3(p_T, p_{T,h})$. If the experimental data is given in terms of the differential multiplicity, the relation

$$\frac{1}{N_{ev}} \frac{1}{2\pi p_{T,K}} \frac{d^2N}{dP_{T,K}dy} = E\frac{d^3\sigma}{d^3p} \frac{1}{\sigma_{tot}} \tag{4.45}$$

with the number of events N_{ev}, number of detected particles N and total cross section σ_{tot}, can be used for comparisons to the theoretical cross section.

5. Analytical Computation of Invariant Matrix Elements

This section investigates and computes the invariant matrix elements at tree-level for the two following processes. First, the annihilation of a massless quark anti-quark pair into a pair of gluons, and secondly, the quark gluon scattering. The results will be given as functions of the Mandelstam variables $\hat{s}, \hat{u}, \hat{t}$, which allow the direct implementation in the cross section derived from the previous section. A detailed calculation is given for the squared invariant amplitude of the t-channel of the first process. The same procedures are applied to the remaining invariant amplitudes. Einstein's summation convention is implied throughout this section along with the Feynman slash notation $\not{p} = \gamma^\mu p_\mu$. The results of all two-to-two parton processes are displayed at the end of this section for further analysis and comparison to experimental data.
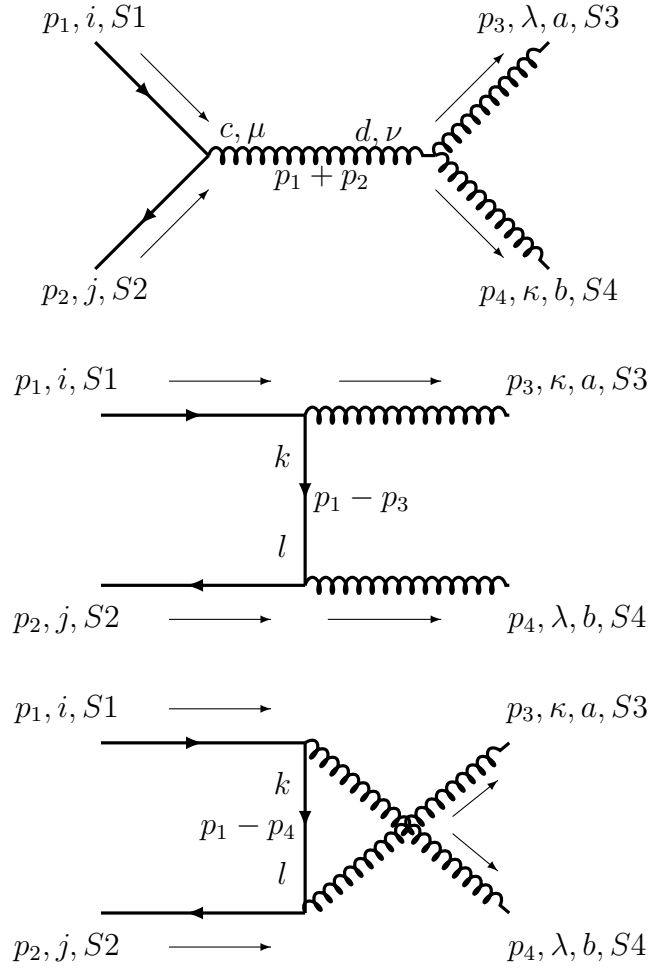
5.1. $q\bar{q} \to gg$

The process

$$q(p_1)\bar{q}(p_2) \to g(p_3)g(p_4)$$

corresponds to the three lowest-order Feynman diagrams shown in fig. 2 for a quark-antiquark annihilation into a gluon-gluon pair. In order to obtain the cross section, the sum over the unobserved final degrees of freedom with corresponding averaging factor for the initial degrees is introduced. Thus, a summation and averaging over polarisation and colour states

$$\overline{\sum} \equiv \frac{1}{N_C^2(2j_q+1)^2} \sum_{pol.} \sum_{col.} \tag{5.1}$$

results, with $N_C = 3$, since colour change would not be detectable, and $j_q = 1/2$ for the polarisation of fermionic quarks. The invariant unpolarized squared amplitude of the s-, t- and u-channels is given by

$$\overline{|\mathcal{M}|^2} = $$
$$\overline{\sum} \left[|\mathcal{M}_s|^2 + |\mathcal{M}_t|^2 + |\mathcal{M}_u|^2 + 2\,\mathrm{Re}\,\mathcal{M}_t^\dagger \mathcal{M}_s + 2\,\mathrm{Re}\,\mathcal{M}_u^\dagger \mathcal{M}_s + 2\,\mathrm{Re}\,\mathcal{M}_t^\dagger \mathcal{M}_u \right]. \tag{5.2}$$

Figure 2: Feynman diagrams (s-, t-, and u-channel) for $\bar{q}q$ annihilation to a pair of gluons.

The invariant amplitudes are labeled with $i, j, k, l = 1, 2, 3$ for quark colour, while indices $a, b, c, d = 1, 2, 3, \ldots, 8$ stand for gluon colours. The corresponding polarisations of the external fermionic and bosonic field are represented by index S. In consideration of a negligible gluon and quark mass, one obtains the following invariant amplitudes for the

tree level Feynman diagrams in fig. 2

$$-i\mathcal{M}_t = -ig_s^2\,\overline{v}_j^{(S2)}(p_2)\,\gamma_\lambda\frac{\slashed{p}_1 - \slashed{p}_3}{(p_1 - p_3)^2}\gamma_\kappa\,u_i^{(S1)}(p_1)\,T_{jl}^b T_{ki}^a \delta_{kl}\,\epsilon_{a,(S3)}^{\kappa*}(p_3)\epsilon_{b,(S4)}^{\lambda*}(p_4) \qquad (5.3)$$

$$-i\mathcal{M}_u = -ig_s^2\,\overline{v}_j^{(S2)}(p_2)\,\gamma_\lambda\frac{\slashed{p}_1 - \slashed{p}_4}{(p_1 - p_4)^2}\gamma_\kappa\,u_i^{(S1)}(p_1)\,T_{jl}^a T_{ki}^b \delta_{kl}\,\epsilon_{a,(S3)}^{\kappa*}(p_3)\epsilon_{b,(S4)}^{\lambda*}(p_4) \qquad (5.4)$$

$$\begin{aligned}-i\mathcal{M}_s = {} & g_s^2\,\overline{v}_j^{(S2)}(p_2)\,\gamma_\mu u_i^{(S1)}(p_1)\,\frac{g^{\mu\nu}}{(p_1 + p_2)^2}\,\delta_{cd}A_{\nu\lambda\kappa}(p_1 + p_2, -p_4, -p_3)\\ & \times f^{dba}T_{ji}^c\,\epsilon_{a,(S3)}^{\kappa*}(p_3)\epsilon_{b,(S4)}^{\lambda*}(p_4)\end{aligned} \qquad (5.5)$$

with Dirac spinors $u_i^{(S1)}\left(\overline{u}_i^{(S1)}\right)$ and $\overline{v}_i^{(S1)}\left(v_i^{(S1)}\right)$ for ingoing (outgoing) particles and antiparticles, respectively, and

$$A_{\nu\lambda\kappa}(p_1, p_2, p_3) \equiv g_{\nu\lambda}(p_1 - p_2)_\kappa + g_{\lambda\kappa}(p_2 - p_3)_\nu + g_{\kappa\nu}(p_3 - p_1)_\lambda \qquad (5.6)$$

resulting from the three-gluon vertex. The completeness relations

$$\sum_S = u^S(p)\overline{u}^S(p) = \slashed{p} + m \qquad (5.7)$$

$$\sum_S = v^S(p)\overline{v}^S(p) = \slashed{p} - m \qquad (5.8)$$

and substitution

$$\sum_S \epsilon_{a,S}^{\lambda*}\epsilon_{a,S}^{\lambda'} \to -g^{\lambda\lambda'} \qquad (5.9)$$

are used when the spinors of the fermions and polarisation vectors of gluons are summed over polarisation S. The calculation of the hermitian conjugate, which is required for the squared matrix elements and interference terms, is shown explicitly for the spinor part of

the t-channel by

$$
\begin{aligned}
&\left[\overline{v}^{(S2)}\, \gamma_\lambda (\slashed{p}_1 - \slashed{p}_3)\gamma_\kappa\, u^{(S1)} \right]^\dagger \\
=&\left[v^{(S2)\dagger}\gamma^0\gamma_\lambda(\slashed{p}_1 - \slashed{p}_3)\gamma_\kappa u^{(S1)} \right]^\dagger \\
=&u^{(S1)\dagger}\gamma_\kappa^\dagger(\slashed{p}_1^\dagger - \slashed{p}_3^\dagger)\gamma_\lambda^\dagger\gamma^{0\dagger}v^{(S2)} \\
=&u^{(S1)\dagger}\gamma^0\gamma_\kappa\gamma^0(\gamma^0\slashed{p}_1\gamma^0 - \gamma^0\slashed{p}_3\gamma^0)\gamma^0\gamma_\lambda\gamma^0\gamma^0 v^{(S2)} \\
=&\overline{u}^{(S1)}\gamma_\kappa(\slashed{p}_1 - \slashed{p}_3)\gamma_\lambda v^{(S2)}
\end{aligned}
\tag{5.10}
$$

with suppression of explicit momentum dependency and colour indices for an improved legibility and with usage of the relations given in eqs. (A.8) to (A.10). Thus, the hermitian conjugated amplitudes

$$
i\mathcal{M}_t^\dagger = ig_s^2\, \overline{u}_i^{(S1)}(p_1)\, \gamma_{\kappa'} \frac{\slashed{p}_1 - \slashed{p}_3}{(p_1 - p_3)^2}\gamma_{\lambda'}\, v_j^{(S2)}(p_2)\, T_{ik'}^a T_{l'j}^b \delta_{k'l'}\, \epsilon_{a,(S3)}^{\kappa'}(p_3)\epsilon_{b,(S4)}^{\lambda'}(p_4)
\tag{5.11}
$$

$$
i\mathcal{M}_u^\dagger = ig_s^2\, \overline{u}_i^{(S1)}(p_1)\, \gamma_{\kappa'} \frac{\slashed{p}_1 - \slashed{p}_4}{(p_1 - p_4)^2}\gamma_{\lambda'}\, v_j^{(S2)}(p_2)\, T_{ik'}^b T_{l'j}^a \delta_{k'l'}\, \epsilon_{a,(S3)}^{\kappa'}(p_3)\epsilon_{b,(S4)}^{\lambda'}(p_4)
\tag{5.12}
$$

$$
\begin{aligned}
i\mathcal{M}_s^\dagger =\ & g_s^2\overline{u}_i^{(S1)}(p_1)\gamma_{\mu'}v_j^{(S2)}(p_2)\frac{g^{\mu'\nu'}}{(p_1 + p_2)^2}\delta_{\tilde{c}\tilde{d}}A_{\nu'\lambda'\kappa'}(p_1 + p_2, -p_4, -p_3) \\
&\times f^{\tilde{d}ba}T_{ij}^{\tilde{c}}\epsilon_{a,(S3)}^{\kappa'}(p_3)\epsilon_{b,(S4)}^{\lambda'}(p_4)
\end{aligned}
\tag{5.13}
$$

follow. The summed, averaged, squared invariant amplitude of the t-channel diagram reads

$$
\begin{aligned}
\overline{\sum}\mathcal{M}_t^\dagger\mathcal{M}_t = \overline{\sum}\ & \frac{g_s^4}{(p_1 - p_3)^4}\epsilon_{a,(S3)}^{\kappa'}(p_3)\epsilon_{b,(S4)}^{\lambda'}(p_4)\, \epsilon_{a,(S3)}^{\kappa*}(p_3)\epsilon_{b,(S4)}^{\lambda*}(p_4) \\
&\times \overline{u}_i^{(S1)}(p_1)\, \gamma_{\kappa'}\left(\slashed{p}_1 - \slashed{p}_3\right)\gamma_{\lambda'}v_j^{(S2)}(p_2)\, \overline{v}_j^{(S2)}(p_2)\, \gamma_\lambda\left(\slashed{p}_1 - \slashed{p}_3\right)\gamma_\kappa\, u_i^{(S1)}(p_1) \\
&\times T_{ik'}^a T_{k'j}^b\, T_{jk}^b T_{ki}^a.
\end{aligned}
\tag{5.14}
$$

For further calculations, it is helpful to decompose the squared matrix element into a product of a term describing colour and a term $L_{\lambda\lambda'\kappa\kappa'}^p$ depending on the momenta. The latter term will be written with explicit matrix indices $\alpha, \beta, \dots$ following [13, p. 122],

which gives

$$
\begin{aligned}
L^p_{\lambda\lambda'\kappa\kappa'} =& \sum_{pol.} \left(\overline{u}^{(S1)}_i(p_1)\right)_\alpha (\gamma_{\kappa'})_{\alpha\beta} \left(\slashed{p}_1 - \slashed{p}_3\right)_{\beta\gamma} (\gamma_{\lambda'})_{\gamma\delta} \left(v^{(S2)}_j(p_2)\right)_\delta \\
& \times \left(\overline{v}^{(S2)}_j(p_2)\right)_\epsilon (\gamma_\lambda)_{\epsilon\zeta} \left(\slashed{p}_1 - \slashed{p}_3\right)_{\zeta\eta} (\gamma_\kappa)_{\eta\theta} \left(u^{(S1)}_i(p_1)\right)_\theta .
\end{aligned}
\tag{5.15}
$$

An application of the completeness relations eqs. (5.7) and (5.8) for massless particles yields

$$
\begin{aligned}
L^p_{\lambda\lambda'\kappa\kappa'} =& \left(\slashed{p}_1\right)_{\theta\alpha} (\gamma_{\kappa'})_{\alpha\beta} \left(\slashed{p}_1 - \slashed{p}_3\right)_{\beta\gamma} (\gamma_{\lambda'})_{\gamma\delta} \left(\slashed{p}_2\right)_{\delta\epsilon} (\gamma_\lambda)_{\epsilon\zeta} \left(\slashed{p}_1 - \slashed{p}_3\right)_{\zeta\eta} (\gamma_\kappa)_{\eta\theta} \\
=& \operatorname{Tr}\left\{\slashed{p}_2\gamma_\lambda(\slashed{p}_1 - \slashed{p}_3)\gamma_\kappa\slashed{p}_1\gamma_{\kappa'}(\slashed{p}_1 - \slashed{p}_3)\gamma_{\lambda'}\right\}.
\end{aligned}
\tag{5.16}
$$

With an additional substitution of the Mandelstam variables $\hat{s} = (p_1 + p_2)^2$, $\hat{t} = (p_1 - p_3)^2$ and $\hat{u} = (p_1 - p_4)^2$ as denominator to emphasize the t-, s- and u-channel character and eq. (5.9), the terms

$$
\sum_S |\mathcal{M}_t|^2 = \frac{g_s^4}{\hat{t}^2} g^{\kappa\kappa'} g^{\lambda\lambda'} \operatorname{Tr}\left\{\slashed{p}_2\gamma_\lambda(\slashed{p}_1 - \slashed{p}_3)\gamma_\kappa\slashed{p}_1\gamma_{\kappa'}(\slashed{p}_1 - \slashed{p}_3)\gamma_{\lambda'}\right\} T^a_{ik'}T^b_{k'j}\,T^b_{jk}T^a_{ki}
\tag{5.17}
$$

$$
\sum_S |\mathcal{M}_u|^2 = \frac{g_s^4}{\hat{u}^2} g^{\lambda\lambda'} g^{\kappa\kappa'} \operatorname{Tr}\left\{\slashed{p}_2\gamma_\kappa(\slashed{p}_1 - \slashed{p}_3)\gamma_\lambda\slashed{p}_1\gamma_{\lambda'}(\slashed{p}_1 - \slashed{p}_3)\gamma_{\kappa'}\right\} T^b_{ik'}T^a_{k'j}\,T^a_{jk}T^b_{ki}
\tag{5.18}
$$

and

$$
\sum_S |\mathcal{M}_s|^2 = \frac{g_s^4}{\hat{s}^2} g^{\kappa\kappa'} g^{\lambda\lambda'} \operatorname{Tr}\left\{\slashed{p}_2\gamma^\mu\slashed{p}_1\gamma^{\mu'}\right\} A_{\nu\lambda\kappa} A^{\nu'\lambda'\kappa'} T^c_{ji} f^{cba} T^{\tilde{c}}_{ij} f^{\tilde{c}ba}
\tag{5.19}
$$

follow accordingly, when summed over the polarisation states. The t-channel can be deducted from the u-channel due to their similar construction (an interchange of p_3 and p_4). Similarly, we obtain the interference terms

$$
\sum_S \mathcal{M}_t^\dagger \mathcal{M}_u = \frac{g_s^4}{\hat{u}\hat{t}} g^{\kappa\kappa'} g^{\lambda\lambda'} \operatorname{Tr}\left\{\slashed{p}_1\gamma_{\kappa'}(\slashed{p}_1 - \slashed{p}_3)\gamma_{\lambda'}\slashed{p}_2\gamma_\lambda(\slashed{p}_1 - \slashed{p}_4)\gamma_\kappa\slashed{p}_1\right\} T^a_{ik'}T^b_{k'j}T^a_{jk}T^b_{ki}
\tag{5.20}
$$

$$
\sum_S \mathcal{M}_t^\dagger \mathcal{M}_s = \frac{g_s^4}{\hat{s}\hat{t}} g^{\kappa\kappa'} g^{\lambda\lambda'} g^{\mu\nu} A_{\nu\lambda\kappa} \operatorname{Tr}\left\{\slashed{p}_1\gamma_{\kappa'}(\slashed{p}_1 - \slashed{p}_3)\gamma_{\lambda'}\slashed{p}_2\gamma_\mu\right\} i T^c_{ji} f^{cba} T^a_{ik} T^b_{kj}
\tag{5.21}
$$

$$
\sum_S \mathcal{M}_u^\dagger \mathcal{M}_s = \frac{g_s^4}{\hat{s}\hat{u}} g^{\kappa\kappa'} g^{\lambda\lambda'} g^{\mu\nu} A_{\nu\lambda\kappa} \operatorname{Tr}\left\{\slashed{p}_1\gamma_{\kappa'}(\slashed{p}_1 - \slashed{p}_4)\gamma_{\lambda'}\slashed{p}_2\gamma_\mu\right\} T^c_{ji} f^{cba} T^b_{ik} T^a_{kj}.
\tag{5.22}
$$

The evaluation of the traces is straight forward and is best done by using the relations given in eqs. (A.1) to (A.5). The t-channel trace from eq. (5.16) is shown explicitly as an example with the metric tensors resulting from the completeness relations. This gives

$$
\begin{aligned}
g^{\kappa\kappa'}g^{\lambda\lambda'}L^p_{\lambda\lambda'\kappa\kappa'} &= g^{\kappa\kappa'}g^{\lambda\lambda'}\operatorname{Tr}\left\{\not{p}_2\gamma_\lambda(\not{p}_1-\not{p}_3)\gamma_\kappa\not{p}_1\gamma_{\kappa'}(\not{p}_1-\not{p}_3)\gamma_{\lambda'}\right\} \\
&= \operatorname{Tr}\left\{\not{p}_2\gamma_\lambda(\not{p}_1-\not{p}_3)\gamma_\kappa\not{p}_1\gamma^\kappa(\not{p}_1-\not{p}_3)\gamma^\lambda\right\} \\
&\overset{eq.\ (A.7)}{=} 4\operatorname{Tr}\left\{\not{p}_2(\not{p}_1-\not{p}_3)\not{p}_1(\not{p}_1-\not{p}_3)\right\} \\
&\overset{eq.\ (A.5)}{=} 32(p_2 p_3)(p_1 p_3) \\
&\overset{eq.\ (4.5)}{=} 8\hat{t}\hat{u}
\end{aligned}
\tag{5.23}
$$

for particles with negligible mass. Due to the summation over the colours, one encounters the following constellations of Gell-Mann matrices $T^a_{ij} = \lambda^a/2$ and structure factors f^{abc} as introduced in section 2.1. The summation over colour with explicitly written summation over repeated indices is straight forward and result in the following relations

$$
\sum_{i,j,a,b}\sum_{k,k'}T^a_{ik'}T^b_{k'j}T^b_{jk}T^a_{ki} = \frac{1}{16}\sum_{a,b}\operatorname{Tr}\left\{\lambda^a\lambda^b\lambda^b\lambda^a\right\} = \frac{16}{3}
\tag{5.24}
$$

$$
\sum_{i,j,a,b}\sum_{c,\tilde{c}}T^c_{ji}T^{\tilde{c}}_{ij}f^{cba}f^{\tilde{c}ba} = \frac{1}{4}\sum_{a,b}\sum_{c,\tilde{c}}f^{cba}f^{\tilde{c}ba}\operatorname{Tr}\left\{\lambda^c\lambda^{\tilde{c}}\right\} = 12
\tag{5.25}
$$

$$
\sum_{i,j,a,b,c}\sum_{k}if^{cba}T^c_{ji}T^b_{ik}T^a_{kj} = \frac{1}{8}\sum_{a,b,c}if^{cba}\operatorname{Tr}\left\{\lambda^c\lambda^b\lambda^a\right\} = -6
\tag{5.26}
$$

$$
\sum_{a,b,i,j}\sum_{k,k'}T^a_{jk}T^b_{ki}T^a_{ik'}T^b_{k'j} = \frac{1}{16}\sum_{a,b}\operatorname{Tr}\left\{\lambda^a\lambda^b\lambda^a\lambda^b\right\} = -\frac{2}{3}.
\tag{5.27}
$$

Finally, one obtains

$$\overline{\sum}|\mathcal{M}_s|^2 = -g_s^4 \frac{2(8\hat{t}^2 + 6\hat{t}\hat{u} + 8\hat{u}^2)}{3\hat{s}^2} \tag{5.28}$$

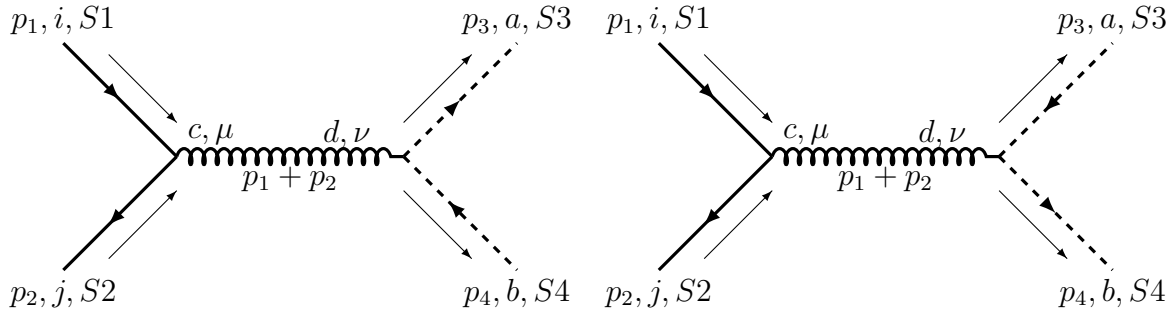$$\overline{\sum}|\mathcal{M}_t|^2 = g_s^4 \frac{32\hat{u}}{27\hat{t}} \tag{5.29}$$

$$\overline{\sum}|\mathcal{M}_u|^2 = g_s^4 \frac{32\hat{t}}{27\hat{u}} \tag{5.30}$$

$$\overline{\sum}2\,\mathrm{Re}\,\mathcal{M}_t^\dagger \mathcal{M}_u = 0 \tag{5.31}$$

$$\overline{\sum}2\,\mathrm{Re}\,\mathcal{M}_t^\dagger \mathcal{M}_s = g_s^4 \frac{4(\hat{s} - \hat{t} + \hat{u})}{3\hat{s}} \tag{5.32}$$

$$\overline{\sum}2\,\mathrm{Re}\,\mathcal{M}_u^\dagger \mathcal{M}_s = g_s^4 \frac{4(\hat{s} + \hat{t} - \hat{u})}{3\hat{s}} \tag{5.33}$$

after the summation over colour and polarisation states, the evaluation of the Dirac traces and inclusion of the averaging factor. The summation in eq. (5.9) considers all polarisation

Figure 3: Feynman diagrams (s-channel) for $\bar{q}q$ annihilation to a ghost-antighost pair $\bar{c}c$.

states, including the non-physical longitudinal polarisation. The summation can be either modified and summed exclusively over physical polarisations, or the introduction of the Fadeev-Popov ghosts (see Feynman diagram fig. 3) is required. They function as correction terms to subtract the non-physical polarisations. The latter approach is chosen in this thesis, which gives

$$\overline{|\mathcal{M}(\bar{q}q \to gg)|^2} = \overline{|\mathcal{M}'(q\bar{q} \to gg)|^2} + \overline{|M_g(q\bar{q} \to c\bar{c})|^2}. \tag{5.34}$$

Because both Feynman diagrams in fig. 3 lead to the same result, we will only evaluate the the left, with the invariant matrix element

$$-i\mathcal{M}_{g,A} = g_s^2 \overline{v}_j^{(S2)}(p_2)\gamma_\mu u_i^{(S1)}(p_1)\frac{g^{\mu\nu}\delta_{cd}}{(p_1+p_2)^2}p_{3,\nu}T_{ji}^c f^{dba} \tag{5.35}$$

$$= \frac{g_s^2}{\hat{s}}\,\overline{v}_j^{(S2)}(p_2)\slashed{p}_3 u_i^{(S1)}(p_1)T_{ji}^c f^{cba}. \tag{5.36}$$

After following the same steps as in the previous calculations

$$\sum_S |\mathcal{M}_{g,A}|^2 = \frac{g_s^4}{\hat{s}^2}\,\mathrm{Tr}\big\{\slashed{p}_2\slashed{p}_3\slashed{p}_1\slashed{p}_3\big\}T_{ji}^c f^{cba}T_{ij}^{\tilde{c}} f^{\tilde{c}ba}, \tag{5.37}$$

and therewith,

$$\overline{|\mathcal{M}_{g,A}|^2} = \overline{\sum}|\mathcal{M}_{g,A}|^2 = -g_s^4\frac{2\hat{u}\hat{t}}{3\hat{s}^2} \tag{5.38}$$

is obtained. The minus sign gets assigned due to the ghost's character as a fermion, because the squared matrix element is represented by a Feynman diagram with a closed fermion loop. At an intuitive level, all unphysical processes are subtracted, so that the resulting cross section is a cross section of physical states only. With the subtraction of longitudinal polarised gluons the final result reads

$$\overline{|\mathcal{M}(qq \to gg)|^2} = \overline{|\mathcal{M}'(q\overline{q} \to gg)|^2} + 2 \cdot \overline{|M_{g,A}(q\overline{q} \to c\overline{c})|^2} \tag{5.39}$$

$$= g_s^4\left[\frac{32}{27}\frac{\hat{t}^2+\hat{u}^2}{\hat{t}\hat{u}} - \frac{8}{3}\frac{\hat{t}^2+\hat{u}^2}{\hat{s}^2}\right], \tag{5.40}$$

which is verified by the results given in [6, p.249].

5.2. $qg \to qg$

The second sub-process of the proton-proton scattering, which is calculated explicitly is

$$q(p_1)g(p_2) \longrightarrow q(p_3)g(p_4)$$

with the corresponding Feynman diagrams at tree level shown in fig. 4. After comparing
to the process in section 5.1, the diagrams of the two sub-processes can be divided into
pairs of two, where the corresponding diagrams are identical when rotated by 90°. Due
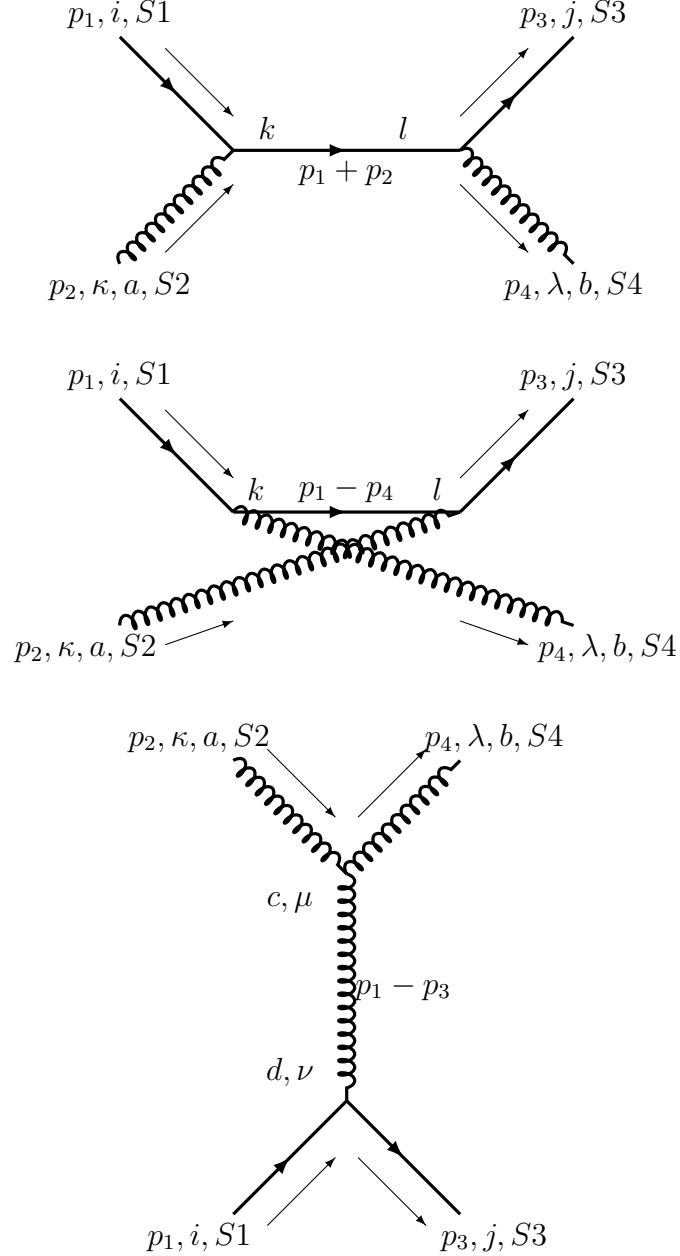
Figure 4: Feynman diagrams (s-, u-, and t-channel) for $qg \to qg$ process.

to the different initial and final states, the averaged sum equals

$$\overline{\sum} \equiv \sum_{pol.} \sum_{col.} \frac{1}{4 \cdot N_C(N_C^2 - 1)} \tag{5.41}$$

with $N_C = 3$. The fermionic quark has 2 polarisation and 3 colour states, which was already used in section 5.1. The gluons, with spin 1 have 2 polarisation states in contrast to massive spin 1 particles, because only the polarisation states transverse to the direction of propagation of a gluon describe physical properties. The squared invariant amplitude reads

$$\overline{|\mathcal{M}|^2} = \\ \overline{\sum} \left[|\mathcal{M}_s|^2 + |\mathcal{M}_t|^2 + |\mathcal{M}_u|^2 + 2\,\text{Re}\,\mathcal{M}_t^\dagger \mathcal{M}_s + 2\,\text{Re}\,\mathcal{M}_u^\dagger \mathcal{M}_s + 2\,\text{Re}\,\mathcal{M}_t^\dagger \mathcal{M}_u \right] \tag{5.42}$$

with

$$-i\mathcal{M}_s = -i\frac{g_s^2}{\hat{s}} \bar{u}_j^{(S3)}(p_3)\gamma_\lambda(\not{p}_1 + \not{p}_2)\gamma_\kappa u_i^{(S1)}(p_1)\delta_{kl}T_{jl}^b T_{ki}^a \epsilon_{b,(S4)}^{\lambda*}(p_4)\epsilon_{a,(S2)}^\kappa(p_2) \tag{5.43}$$

$$-i\mathcal{M}_u = -i\frac{g_s^2}{\hat{u}} \bar{u}_j^{(S3)}(p_3)\gamma_\kappa(\not{p}_1 - \not{p}_4)\gamma_\lambda u_i^{(S1)}(p_1)\delta_{kl}T_{jl}^a T_{ki}^b \epsilon_{b,(S4)}^{\lambda*}(p_4)\epsilon_{a,(S2)}^\kappa(p_2) \tag{5.44}$$

$$-i\mathcal{M}_t = \frac{g_s^2}{\hat{t}} \bar{u}_j^{(S3)}(p_3)\gamma_\nu u_i^{(S1)}(p_1)g^{\nu\mu}\delta_{cd}A_{\kappa\mu\nu}(p_2, p_1 - p_3, -p_4) \\ \times f^{abc}T_{ji}^d \epsilon_{b,(S4)}^{\lambda*}(p_4)\epsilon_{a,(S2)}^\kappa(p_2). \tag{5.45}$$

The Lorentz tensor is defined in eq. (5.6). We once again sum over all polarisation states, which leads to the evaluation of the Dirac-traces from

$$\sum_S |\mathcal{M}_s|^2 = \frac{g_s^4}{\hat{s}^2} g^{\lambda\lambda'} g^{\kappa\kappa'} \text{Tr}\left\{ \not{p}_3\gamma_\lambda(\not{p}_1 + \not{p}_2)\gamma_\kappa \not{p}_1 \gamma_{\kappa'}(\not{p}_1 + \not{p}_2)\gamma_{\lambda'} \right\} T_{jk}^b T_{ki}^a T_{ik'}^a T_{k'j}^b \tag{5.46}$$

$$\sum_S |\mathcal{M}_u|^2 = \frac{g_s^4}{\hat{u}^2} g^{\lambda\lambda'} g^{\kappa\kappa'} \text{Tr}\left\{ \not{p}_3\gamma_\kappa(\not{p}_1 - \not{p}_4)\gamma_\lambda \not{p}_1 \gamma_{\lambda'}(\not{p}_1 - \not{p}_4)\gamma_{\kappa'} \right\} T_{jk}^a T_{ki}^b T_{ik'}^b T_{k'j}^a \tag{5.47}$$

$$\sum_S |\mathcal{M}_t|^2 = \frac{g_s^4}{\hat{t}^2} g^{\lambda\lambda'} g^{\kappa\kappa'} \text{Tr}\left\{ \not{p}_3\gamma_\nu \not{p}_1 \gamma_{\nu'} \right\} g^{\mu\nu} g^{\mu'\nu'} A_{\kappa\mu\nu} A^{\kappa'\mu'\nu'} f^{abc}T_{ji}^c f^{ab\tilde{c}}T_{ij}^{\tilde{c}} \tag{5.48}$$

for the squared and

$$\sum_S \mathcal{M}_s^\dagger \mathcal{M}_u = \frac{g_s^4}{\hat{s}\hat{u}} g^{\lambda\lambda'} g^{\kappa\kappa'} \text{Tr}\Big\{ \slashed{p}_1 \gamma_{\kappa'} (\slashed{p}_1 + \slashed{p}_2) \gamma_{\lambda'} \slashed{p}_3 \gamma_\kappa (\slashed{p}_1 - \slashed{p}_4) \gamma_\lambda \Big\} T_{jk}^a T_{ki}^b T_{ik'}^a T_{k'j}^b \tag{5.49}$$

$$\sum_S \mathcal{M}_s^\dagger \mathcal{M}_t = \frac{g_s^4}{\hat{s}\hat{t}} g^{\lambda\lambda'} g^{\kappa\kappa'} \text{Tr}\Big\{ \slashed{p}_1 \gamma_{\kappa'} (\slashed{p}_1 + \slashed{p}_2) \gamma_{\lambda'} \slashed{p}_3 \gamma_\nu \Big\} g^{\mu\nu} A_{\kappa\mu\nu} i f^{abc} T_{ji}^c T_{ik'}^a T_{k'j}^b \tag{5.50}$$

$$\sum_S \mathcal{M}_u^\dagger \mathcal{M}_t = \frac{g_s^4}{\hat{t}\hat{u}} g^{\lambda\lambda'} g^{\kappa\kappa'} \text{Tr}\Big\{ \slashed{p}_1 \gamma_{\lambda'} (\slashed{p}_1 - \slashed{p}_4) \gamma_{\kappa'} \slashed{p}_3 \gamma_\nu \Big\} g^{\mu\nu} A_{\kappa\mu\nu} i f^{abc} T_{ji}^c T_{ik'}^b T_{k'j}^a \tag{5.51}$$

for the crossed terms. The colour factors were already calculated in eqs. (5.24) to (5.27) and the Dirac traces can be taken from section 5.1, with an interchange of corresponding momenta due to the relation of the diagrams through a 90° rotation.
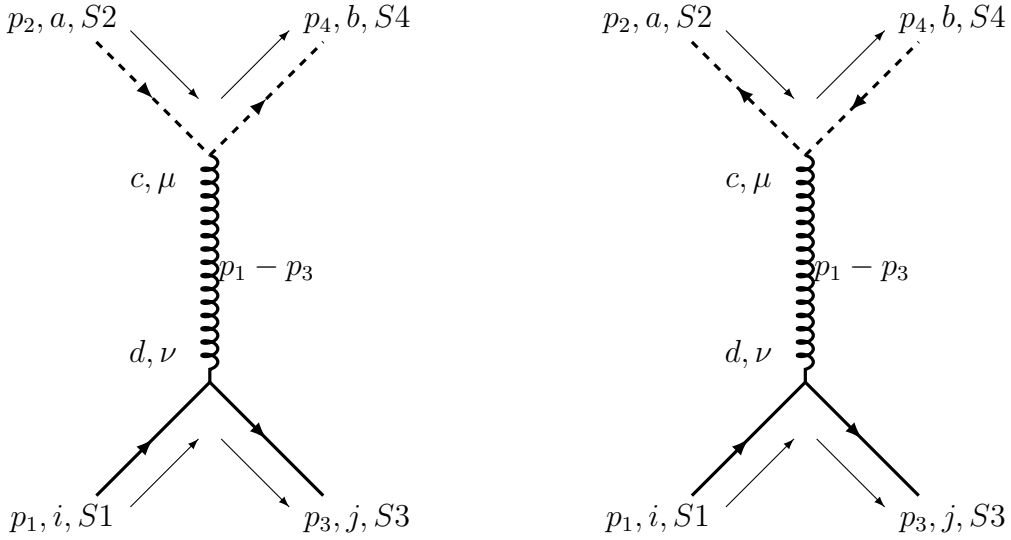
Figure 5: Feynman diagrams (s-channel) for $qc \to qc$ and $q\bar{c} \to q\bar{c}$ process.

Since the substitution eq. (5.9) with summation over all polarisation states includes non-physical states, the Faddeev-Popov ghost are introduced. The invariant matrix

element reads

$$-i\mathcal{M}_{g,A'} = -ig_s^2 \overline{u}_j^{(S3)}(p_3)\gamma_\nu u_i^{(S1)}(p_1)\frac{g^{\mu\nu}\delta_{cd}}{(p_1+p_2)^2}p_{4,\mu}f^{cba}T_{ji}^d$$

$$= \frac{g_s^2}{\hat{s}}\overline{u}_j^{(S3)}(p_3)\slashed{p}_4 u_i^{(S1)}(p_1)f^{cab}T_{ji}^c \tag{5.52}$$

$$\Rightarrow \sum_S |\mathcal{M}_{g,A'}|^2 = \frac{g_s^4}{\hat{s}^2}\,\mathrm{Tr}\big\{\slashed{p}_3\slashed{p}_4\slashed{p}_1\slashed{p}_4\big\}f^{cab}f^{\tilde{c}ba}T_{ji}^c T_{ij}^{\tilde{c}}.$$

Both Feynman diagrams containing the Faddeev-Popov ghosts lead to the same results, therefore we only study the left diagram. The calculation is carried out as described in the previous section, which involves Dirac traces, the averaging factor and the summation over colour and polarisation states. This leads to the following results

$$\overline{\sum}|\mathcal{M}_s|^2 = -g_s^4\frac{4\hat{u}}{9\hat{s}} \tag{5.53}$$

$$\overline{\sum}|\mathcal{M}_u|^2 = -g_s^4\frac{4\hat{s}}{9\hat{u}} \tag{5.54}$$

$$\overline{\sum}|\mathcal{M}_t|^2 = g_s^4\frac{8\hat{t}^2 + 10\hat{t}\hat{u} + 10\hat{u}^2}{4\hat{t}^2} \tag{5.55}$$

$$\overline{\sum}2\,\mathrm{Re}\,\mathcal{M}_s^\dagger\mathcal{M}_u = 0 \tag{5.56}$$

$$\overline{\sum}2\,\mathrm{Re}\,\mathcal{M}_s^\dagger\mathcal{M}_t = g_s^4\frac{\hat{s}}{\hat{t}} \tag{5.57}$$

$$\overline{\sum}2\,\mathrm{Re}\,\mathcal{M}_u^\dagger\mathcal{M}_t = g_s^4\frac{\hat{u}}{\hat{t}} \tag{5.58}$$

$$\overline{\sum}|\mathcal{M}_{g,A'}| = -g_s^4\frac{\hat{s}\hat{u}}{4\hat{t}^2} \tag{5.59}$$

and the invariant matrix element squared

$$\overline{|\mathcal{M}(qg\to qg)|^2} = \overline{|\mathcal{M}'(qg\to qg)|^2} + 2\cdot\overline{|M_{g,A'}(qc\to qc)|^2} \tag{5.60}$$

$$= g_s^4\left[\frac{\hat{s}^2+\hat{u}^2}{\hat{t}^2} - \frac{4(\hat{s}^2+\hat{u}^2)}{9\hat{s}\hat{u}}\right]. \tag{5.61}$$

This result coincides with the cross section given in [6, p. 249]. A summary of matrix elements squared for all two-to-two parton sub-processes is given in table 1.

Table 1: Invariant matrix elements squared for all two-to-two parton sub-processes for massless partons, taken from [6, p. 249]

Process	$\overline{\sum}|\mathcal{M}|^2/g_s^4$
$qq' \to qq'$	$\dfrac{4}{9}\dfrac{\hat{s}^2 + \hat{u}^2}{\hat{t}^2}$
$q\overline{q'} \to q\overline{q'}$	$\dfrac{4}{9}\dfrac{\hat{s}^2 + \hat{u}^2}{\hat{t}^2}$
$qq \to qq$	$\dfrac{4}{9}\left(\dfrac{\hat{s}^2 + \hat{u}^2}{\hat{t}^2} + \dfrac{\hat{s}^2 + \hat{t}^2}{\hat{u}^2}\right) - \dfrac{8}{27}\dfrac{\hat{s}^2}{\hat{u}\hat{t}}$
$q\overline{q} \to q'\overline{q'}$	$\dfrac{4}{9}\dfrac{\hat{t}^2 + \hat{u}^2}{\hat{s}^2}$
$q\overline{q} \to q\overline{q}$	$\dfrac{4}{9}\left(\dfrac{\hat{s}^2 + \hat{u}^2}{\hat{t}^2} + \dfrac{\hat{t}^2 + \hat{u}^2}{\hat{s}^2}\right) - \dfrac{8}{27}\dfrac{\hat{u}^2}{\hat{s}\hat{t}}$
$q\overline{q} \to gg$	$\dfrac{32}{27}\dfrac{\hat{t}^2 + \hat{u}^2}{\hat{t}\hat{u}} - \dfrac{8}{3}\dfrac{\hat{t}^2 + \hat{u}^2}{\hat{s}^2}$
$gg \to q\overline{q}$	$\dfrac{1}{6}\dfrac{\hat{t}^2 + \hat{u}^2}{\hat{t}^2\hat{u}^2} - \dfrac{3}{8}\dfrac{\hat{t}^2 + \hat{u}^2}{\hat{s}^2}$
$gq \to gq$	$-\dfrac{4}{9}\dfrac{\hat{s}^2 + \hat{u}^2}{\hat{s}\hat{u}} + \dfrac{\hat{u}^2 + \hat{s}^2}{\hat{t}^2}$
$gg \to gg$	$\dfrac{9}{2}\left(3 - \dfrac{\hat{t}\hat{u}}{\hat{s}^2} - \dfrac{\hat{s}\hat{u}}{\hat{t}^2} - \dfrac{\hat{s}\hat{t}}{\hat{u}^2}\right)$

6. Numerical Results and Comparison with Experiment

This section provides a comparison between the predicted multiplicity and the experimental data for a $pp \rightarrow (K^+ + K^-)X$ process at $\sqrt{s} = 2.76\,\text{TeV}$ taken from [1]. To obtain the graph of the QCD predicted cross section, eq. (4.44) has to be computed, which leaves a dependency on the parameters $P_{T,K}$, y_4 and s. In this experimental setup the centre-of-mass energy of the colliding protons is determined to be $\sqrt{s} = 2.76\,\text{GeV}$ and the kaons are measured at central rapidity $y_4 \leq |0.8|$. The chosen scales are $Q = \sqrt{s}$ and $\mu = p_T$.

The summation over relevant quark and gluon combinations follows directly from $K^+ = |u\bar{s}\rangle$ and $K^- = |s\bar{u}\rangle$. Equations eq. (2.46) and eq. (2.47) show that the coupling constant $\alpha_s(Q^2)$ is sufficiently small, which justifies the application of perturbative QCD (pQCD). The integration in eq. (4.44) is executed numerically via the Monte Carlo method. The Monte Carlo integration for definite integrals is based on the ratio of the total number of randomly (or pseudo-randomly) generated points in a simple domain D containing the integrated area A and the number of points which are inside of the boundaries of A. The usage of the *VEGAS* algorithm improves the estimated integral and simplifies the computation through a variable transformation, which flattens the integrand [17]. It turns out to be beneficial to introduce the new variables $r_{1/2} \in [0,1]$, which leads to

$$p_T = \left(\frac{\sqrt{s}}{2} - P_{T,Kaon} \right) \cdot r_1 + P_{T,Kaon} \tag{6.1}$$

$$y_3 = 2 \cdot \operatorname{arcosh}\left(\frac{\sqrt{s}}{p_T} - \cosh y_4 \right) \cdot r_2 - \operatorname{arcosh}\left(\frac{\sqrt{s}}{p_T} - \cosh y_4 \right). \tag{6.2}$$

With substitution of the variables $r_{1/2}$ in eq. (4.44) the integral reads

$$
\begin{aligned}
\frac{d^2\sigma}{dP_{T,Kaon}dy_4} = {} & \int_0^1 dr_1 \cdot \left(\frac{\sqrt{s}}{2} - P_{T,Kaon} \right) \int_0^1 dr_2 \cdot 2\operatorname{arcosh}\left(\frac{\sqrt{s}}{p_T(r_1)} - \cosh y_4 \right) \\
& \times \frac{1}{16\pi\tau s^2} \sum_{i,j,k,l=q,\bar{q},g} f_i(x_1,Q^2) f_j(x_2,Q^2) D_{Kaon/k}(x_3,\mu^2) \\
& \times \overline{\sum} |\mathcal{M}_{ij\rightarrow kl}|^2 \frac{1}{1+\delta_{ij}} \frac{1}{1+\delta_{kl}}.
\end{aligned}
\tag{6.3}
$$

The parton density functions $f_i(x, Q^2)$ are supplied by the LHAPDF library [3]. The implementation of the PDF's is done via the python interface of version LHAPDF-6.3.0 and usage of the central set *CT10*. The fragmentation function $D_{Kaon/k}(x_3, \mu^2)$ for unpolarised cross sections is given by de Florian et. al. in [4, 5, 7] for $x_3 \geq 0.05$ and $\mu \geq 1\,\text{GeV}$. Discrete data points of the total cross section σ_{tot} shown in fig. 6 are extracted with the program *Graph Grabber*[10]. A function of the form
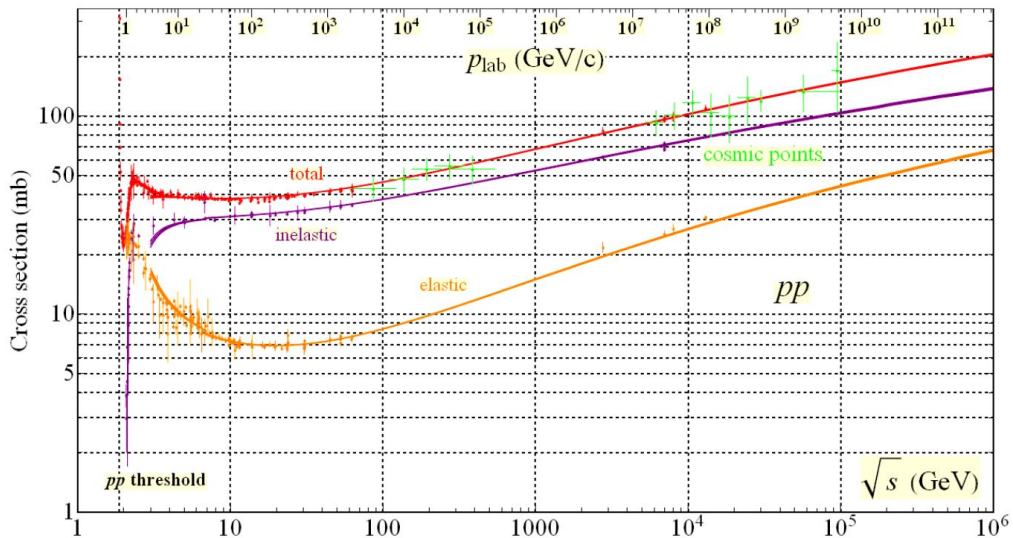
$$\sigma_{fit}(x) = a_0 \cdot \ln^2 x + a_1 \cdot \ln x + a_3 \tag{6.4}$$

is fitted to the series of data points of the total cross section for $\sqrt{s} = 3.5, \dots, 770044\,\text{GeV}$ following [9, p. 22], where $x = \sqrt{s}$ with $a_0 = (1.15 \pm 0.01)\,\text{mb}$, $a_1 = (-3.90 \pm 0.09)\,\text{mb}$ and
$a_2 = (41.24 \pm 0.32)\,\text{mb}$. Hence, the total cross section of a proton-proton collision at $\sqrt{s} = 2760\,\text{GeV}$ is

$$\sigma_{tot,fit}(2760\,\text{GeV}) = (82.41 \pm 0.88)\,\text{mb}, \tag{6.5}$$

which allows the conversion between cross section and multiplicity according to eq. (4.45).

Figure 6: Total, elastic and inelastic cross sections for proton-proton collisions, as function of laboratory beam momentum and total centre-of-mass energy, taken from [11, p. 705].

The resulting p_T distribution of the $K^+ + K^-$ production, measured in *pp* collisions at $\sqrt{s} = 2.76 \, \text{TeV}$ for $y \leq |0.8|$, is shown in fig. 7. The experimental data points are taken from Betty Bezverkhny Abelev et al. [1].

The blue curve is the QCD prediction in first order perturbation theory at $\mathcal{O}(\alpha_s^2)$. The smallest relative deviation from the predicted multiplicity to the given data is observed for $p_T < 5$ GeV. The predicted curve lies above the data points, with the exception for $1.5 \, \text{GeV} \leq p_T \leq 3.5 \, \text{GeV}$. The quotient of the experimental data and theoretical prediction decreases for large p_T. The quotient of the data and prediction shows that the predicted multiplicity is in the order of magnitude of the experimental data. Therefore, this comparison provides a sanity check for the agreement of the theoretical framework used to describe the particle production in a hadron-hadron collision and the experimental data.
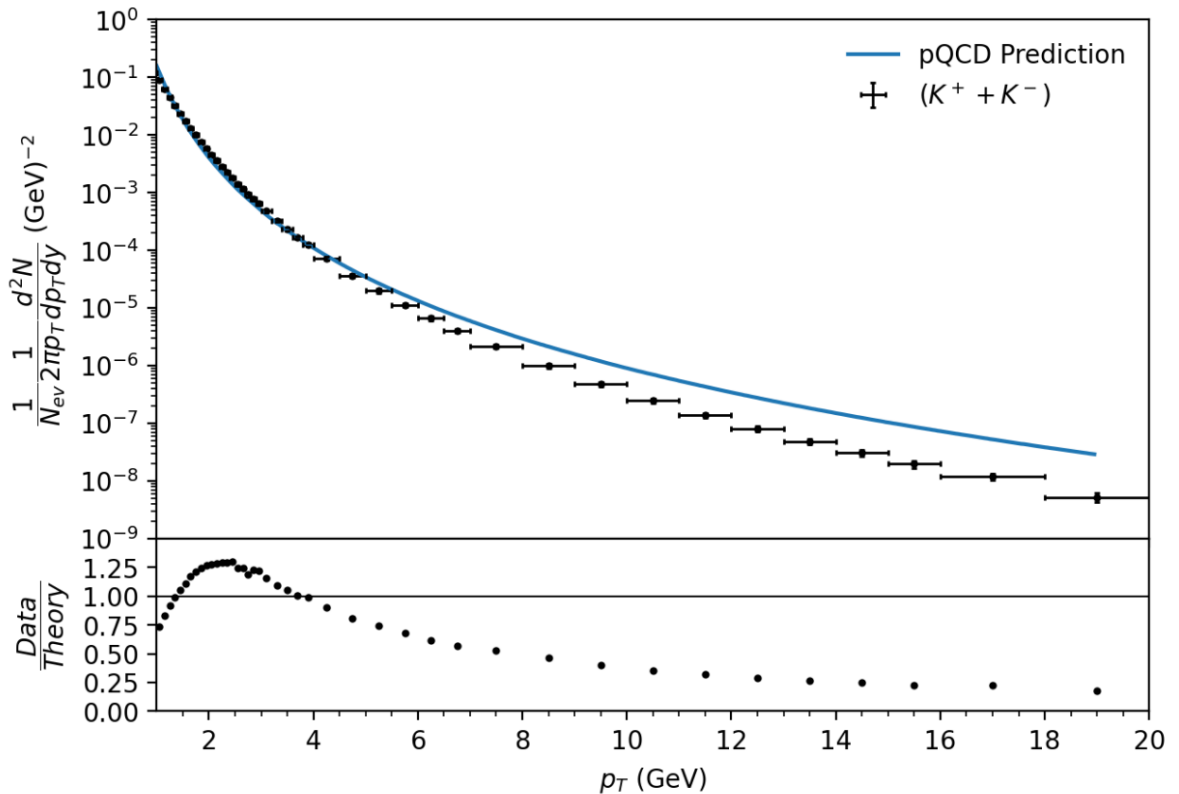
Figure 7: Cross section p_T distribution of a charged kaon production in proton-proton collisions at $\sqrt{s} = 2.76 \, \text{TeV}$ from the ALICE collaboration [1], compared with a leading order QCD prediction.

The predicted fractional contributions of the two-to-two sub-processes is shown in fig. 8. The probability of a charged kaon being the outcome of the dominating $gg \to gg$ process decreases for increasing p_T from 90% to 64% for $p_T = 1, \dots, 19\,\mathrm{GeV}$. The $qg \to qg$ process is the second most important, with a fractional contribution increasing from 6% to 26%. The remaining processes contribute therefore 4% to 10% to the charged kaon production.
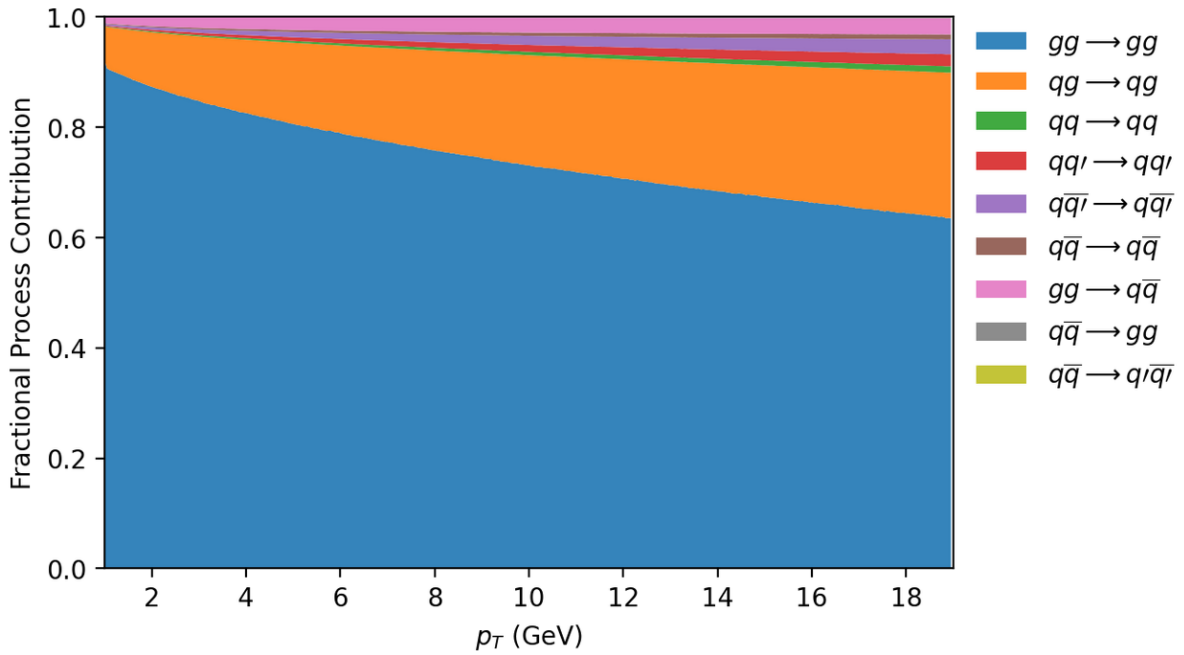
Figure 8: Fraction of the charged kaon production for the two-to-two processes as a function of p_T.

7. **Conclusion and Outlook**

In this thesis, we have studied the particle production in hadron-hadron collisions in leading order of perturbative QCD. A short introduction to the underlying theoretical background is followed by a discussion of cross sections and the explicit calculation of two matrix elements of the two-to-two sub-processes in hadron-hadron collisions. The numerical evaluation in section 6 has succeeded in showing the agreement on the experimental data with the predicted behaviour of the cross section in order of magnitude as a function of the transverse momentum p_T. This is followed by the presentation of the predicted fractional contribution of all two-to-two processes depending on p_T, while $gg \to gg$ and $qg \to qg$ are the most contributing processes.

Further research on the calculation of the invariant matrix elements is suggested, since this thesis only considers the tree-level matrix elements. An improvement in the agreement between the prediction and the experimental data can be achieved by the computation of higher order correction terms in perturbation theory. The next-to-leading order correction consists of virtual corrections (virtual loops including the incorporation of UV renormalisation), real corrections (radiation of extra particles relative to leading order) and subtraction terms arising from infrared singularities [14, p. 38]. The strong dependency of the PDF's and fragmentation function on the scale factors in leading order calculations can be mitigated by the inclusion of higher order terms. Additionally, further analysis can be accompanied with the discussion of the uncertainties caused by the PDF's and the fragmentation function. The computation of the uncertainties was neglected due to the extensive computation time.

A. Appendix

A.1. Dirac Traces

The calculation of the trace of Dirac matrices can be simplified when the following relations taken from [13, p. 123] are applied

$$\text{Tr}\{\gamma^{\nu_1}\cdots\gamma^{\nu_{2k+1}}\} = 0 \quad k \in \mathbb{N}_0 \tag{A.1}$$

$$\text{Tr}\{\gamma^\nu\gamma^\mu\} = 4g^{\nu\mu} \tag{A.2}$$

$$\text{Tr}\{\gamma^\nu\gamma_\mu\} = 16 \tag{A.3}$$

$$\text{Tr}\{\gamma^\nu\gamma_\mu\gamma^\rho\gamma^\sigma\} = 4\left[g^{\nu\mu}g^{\rho\sigma} - g^{\nu\rho}g^{\mu\sigma} + g^{\nu\sigma}g^{\mu\rho}\right] \tag{A.4}$$

$$\text{Tr}\{\displaystyle{\not{a}\not{b}\not{c}\not{d}}\} = 4\left[(a\cdot b)(c\cdot d) - (a\cdot c)(b\cdot d) + (a\cdot d)(b\cdot c)\right] \tag{A.5}$$

$$\gamma_\mu\gamma^\mu = 4 \tag{A.6}$$

$$\gamma_\mu\not{a}\gamma^\mu = -2\not{a}. \tag{A.7}$$

A.2. Dirac Matrices

Dirac matrices γ^μ obey the Clifford algebra

$$\frac{1}{2}\{\gamma^\mu, \gamma^\nu\} \equiv \frac{1}{2}(\gamma^\mu\gamma\nu + \gamma^\nu\gamma\mu) = g^{\mu\nu}\mathbb{1} \tag{A.8}$$

$$\gamma^{\mu\dagger} = \gamma^0\gamma^\mu\gamma^0, \tag{A.9}$$

and therefore,

$$(\gamma^0)^2 = -(\gamma^i)^2 = \mathbb{1}, \quad \gamma^{0\dagger} = \gamma^0, \quad \gamma^{i\dagger} = -\gamma^i. \tag{A.10}$$

References

[1] Betty Bezverkhny Abelev et al. *Production of charged pions, kaons and protons at large transverse momenta in pp and Pb-Pb collisions at $\sqrt{s_{NN}}$ =2.76 TeV*. Vol. 736. 2014, pp. 196–207. DOI: `10.1016/j.physletb.2014.07.011`. arXiv: `1401.1250` `[nucl-ex]`.

[2] Y. Aharonov and D. Bohm. *Significance of Electromagnetic Potentials in the Quantum Theory*. Vol. 115. American Physical Society, Aug. 1959, pp. 485–491. DOI: `10.1103/PhysRev.115.485`.

[3] Andy Buckley et al. *LHAPDF6: parton density access in the LHC precision era*. Vol. 75. 3. Springer Science and Business Media LLC, Mar. 2015. DOI: `10.1140/epjc/s10052-015-3318-8`.

[4] M. Stratmann D. de Florian R. Sassot. *Global analysis of fragmentation functions for pions and kaons and their uncertainties*. 2007. DOI: `10.1103/PhysRevD.75.114010`.

[5] M. Stratmann D. de Florian R. Sassot. *Global analysis of fragmentation functions for protons and charged hadrons*. 2007. DOI: `10.1103/PhysRevD.76.074033`.

[6] R. K. Ellis, W. J. Stirling, and B. R. Webber. *QCD and Collider Physics*. Cambridge Monographs on Particle Physics, Nuclear Physics and Cosmology. Cambridge University Press, 1996. DOI: `10.1017/CBO9780511628788`.

[7] D. de Florian et. al. *Parton-to-Pion Fragmentation Reloaded*. 2014. DOI: `10.1103/PhysRevD.91.014035`.

[8] Harald Fritzsch. *Quantenfeldtheorie - Wie man beschreibt, was die Welt im Innersten zusammenhält*. Springer-Verlag Berlin Heidelberg, 2015, pp. 155–161. DOI: `10.1007/978-3-662-45246-2`.

[9] I. Atanassov et al. G. Antchev. *First determination of the ρ parameter at $\sqrt{s} = 13$ TeV: probing the existence of a colourless C-odd three-gluon compound state*. Vol. 785. 2019. DOI: `doi.org/10.1140/epjc/s10052-019-7223-4`.

[10] *Graph Grabber 2.0.2*. 2020. URL: `www.quintessa.org/software/downloads-and-demos/graph-grabber-2.0.2`.

[11] Particle Data Group and P.A. Zyla et al. *Review of Particle Physics*. Vol. 2020. 8. Aug. 2020. DOI: `10.1093/ptep/ptaa104`.

[12] Brian C. Hall. *Quantum Theory for Mathematicians*. Graduate Texts in Mathematics 267. Springer-Verlag New York, 2013. ISBN: 978-1-4614-7115-8,978-1-4614-7116-5.

[13] Francis Halzen and Alan Martin. *Quarks & Leptons: An introductory course in modern particle physics*. John Wiley & Sons, 1984.

[14] Gudrun Heinrich. *Colourful Loops: Introduction to Quantum Chromodynamics and Loop Calculations*. Max Planck Institute for Physics, Munich, 2018.

[15] H. Honkanen K.J. Eskola. *A perturbative QCD analysis of charged-particle distributions in hadronic and nuclear collisions*. 2003, pp. 167–187. DOI: `10.1103/PhysRevD.91.014035`.

[16] Oliver Ledwig. *Next-to-leading order QCD corrections to the Drell-Yan process*. Westfälische Wilhelms-Universität Münster, 2017.

[17] G. Peter Lepage. *A new algorithm for adaptive multidimensional integration*. Vol. 27. 2. May 1978, pp. 192–203. DOI: `10.1016/0021-9991(78)90004-9`.

[18] Michelangelo L. Mangano. *Introduciton to QCD*. CERN, TH Division, 1998.

[19] Prof. Dr. Gernot Münster. *Von der Quantenfeldtheorie zum Standardmodell-Eine Einführung in die Teilchenphysik*. 2019, pp. 190–206, 237–238. DOI: `10.1515/9783110638547`.

[20] C. Patrignani et al. *Review of Particle Physics*. Vol. 40. 2016. DOI: `10.1088/1674-1137/40/10/100001`.

[21] Lewis H. Ryder. *Quantum Field Theory*. Vol. 2. Cambridge University Press, 1996. ISBN: 978-0-521-47814-4.

[22] L. Van Hove. *Particle production in high energy hadron collisions*. Vol. 1. 7. 1971, pp. 347–379. DOI: `https://doi.org/10.1016/0370-1573(71)90013-5`. URL: `http://www.sciencedirect.com/science/article/pii/0370157371900135`.